Moments of proton GPDs from the OPE of nonlocal quark bilinears up to NNLO

Shohini Bhattacharya, ¹ Krzysztof Cichy, ² Martha Constantinou, ³ Xiang Gao, ^{4,*} Andreas Metz, ³ Joshua Miller, ³ Swagato Mukherjee, ⁵ Peter Petreczky, ⁵ Fernanda Steffens, ⁶ and Yong Zhao, ¹RIKEN BNL Research Center, Brookhaven National Laboratory, Upton, New York 11973, USA, ²Faculty of Physics, Adam Mickiewicz University, ul. Uniwersytetu Poznańskiego 2, 61-614 Poznań, Poland, ³Department of Physics, Temple University, Philadelphia, Pennsylvania 19122-1801, USA, ⁴Physics Division, Argonne National Laboratory, Lemont, Illinois 60439, USA, ⁵Physics Department, Brookhaven National Laboratory, Upton, New York 11973, USA, ⁶Institut für Strahlen- und Kernphysik, Rheinische Friedrich-Wilhelms-Universität Bonn, Nussallee 14-16, 53115 Bonn, Germany

(Received 22 May 2023; accepted 7 July 2023; published 17 July 2023)

For the first time, we present a lattice QCD determination of Mellin moments of unpolarized generalized parton distributions (GPDs) of the proton from an analysis of the quasi-GPD matrix elements within the short-distance factorization framework. We perform our calculation on an $N_f = 2 + 1 + 1$ twisted mass fermions ensemble with a clover improvement at lattice spacing a = 0.093 fm and a pion mass of $m_{\pi} = 260$ MeV. Focusing on the zero-skewness case, the isovector and isoscalar quasi-GPDs are calculated from the γ_0 definition, as well as a recently proposed Lorentz-invariant definition. We utilize data on both symmetric and asymmetric kinematic frames, which allows us to obtain the Mellin moments for several values of the momentum transfer, -t, in the range 0.17 to 2.77 GeV². We use the ratio scheme for GPDs, i.e. renormalization group invariant ratios with leading-twist factorization formula and perturbatively calculated matching coefficients up to the next-next-to-leading order (NNLO) to extract Mellin moments of GPDs, which are consistent with renormalization-group improved results. We compare our determination from quasi-GPDs with the results extracted using standard calculations of Mellin moments of local operators, specifically those related to the electromagnetic and gravitational form factors. We estimated the moments of GPDs up to the fifth ones for the first time. By extrapolating the Mellin moments to -t = 0, we obtained the quark charges, momentum fraction, as well as the angular momentum contributions to the proton spin. The impact parameter space interpretation of the GPD moments is discussed, which provides insights into the spatial distribution of unpolarized quarks and their correlations in the transverse plane of an unpolarized or transversely polarized proton.

DOI: 10.1103/PhysRevD.108.014507

I. INTRODUCTION

The introduction of generalized parton distributions (GPDs) [1–3] has opened up a new perspective into the three-dimensional imaging of the nucleon. These pioneering quantities reveal information on hadron structure far beyond the traditional one-dimensional parton distribution functions (PDFs), typically investigated in deep-inelastic scattering (DIS) experiments, and the transverse structure

Published by the American Physical Society under the terms of the Creative Commons Attribution 4.0 International license. Further distribution of this work must maintain attribution to the author(s) and the published article's title, journal citation, and DOI. Funded by SCOAP³. encoded in the various form factors. In particular, GPDs provide a more comprehensive and nuanced view of the internal structure of the nucleon, offering insights into the spatial distributions of quarks and gluons [4–7]. What is more, the moments of GPDs are related to the matrix elements of the energy-momentum tensor (EMT), from which we can gain valuable insights into the distribution of the hadron's internal energy, momentum, and pressure [8–10], as well as the coupling of hadrons to gravity. Extracting the moments at zero momentum transfer allows the momentum fraction, spin, and angular momentum carried by the quarks and gluons inside the hadron to be determined. These information have the potential to improve our understanding of fundamental physics and could lead to significant advancements in various fields within nuclear and particle physics.

^{*}gaox@anl.gov

There have been efforts to parametrize the GPDs and fit them from global experiments [8,11–21], but this field is still in its infancy, as it remains a challenge to extract the *x*-dependence of GPDs from processes such as deeply virtual Compton scattering (DVCS) [22–25]. Other exclusive reactions, which could in principle alleviate this problem, include double DVCS [26,27] and further processes where two particles (with one or both of them being photons) are detected in addition to the final-state nucleon [28–32]. However, those are typically very difficult to measure. Given the challenges in extracting GPDs from experiments, it is highly desirable to have lattice QCD results that provide complementary knowledge and potential guidance to experiments.

In this work, we focus on the GPDs with unpolarized quarks, H and E, which are obtained from the Fourier transform of light-cone correlators

$$F^{\mu}(z, P, \Delta) = \langle p_f | \bar{q} \left(-\frac{z}{2} \right) \gamma^{\mu} \mathcal{W} \left(-\frac{z}{2}, \frac{z}{2} \right) q \left(\frac{z}{2} \right) | p_i \rangle, \quad (1)$$

with $\gamma^{\mu}=\gamma^+$. The quark and antiquark are separated along the light-cone direction $z=ln_-$ and are connected by the Wilson-line $W(-\frac{z}{2},\frac{z}{2})=\mathcal{P}\exp(i\int_{-ln_-/2}^{ln_-/2}dl'A^+)$. Because of Lorentz invariance, the GPDs are functions of x and two Lorentz-invariant products of the vectors p_f , p_i^{-1} and n_- , which is conventionally chosen as $\xi=-(\Delta n_-)/(2Pn_-)$ and $t=\Delta^2$. Though lattice QCD can compute nonperturbative matrix elements, these are time-dependent quantities and cannot be computed for a lattice defined in Euclidean space. It is instead the first few Mellin moments of GPDs that are traditionally extracted from the lattice [33–52], as matrix elements of local operators. However, due to signal decay and power-divergent mixing under renormalization, there are no moments beyond the third that exist.

Breakthrough was made about a decade ago when the quasi-PDF method was proposed [53,54] that utilizes operators holding the same form as Eq. (1) but with equaltime quark fields that are separated along a spatial direction. Without loss of generality, the direction is chosen to be $z = ln_3$. This approach paves a way to relate the Euclidean matrix elements to the light-cone PDFs through factorization by an expansion in powers of $1/P_3$, with P_3 the hadron momentum, and makes it possible to compute x-dependent PDFs from lattice QCD. The quasi-PDF approach, often referred to as large momentum effective theory (LaMET) [55], was then extended to the GPDs and other light-cone quantities. Starting from the same quasi-PDF operator, the so-called Ioffe-time pseudodistributions or pseudo-PDFs (pPDFs) [56,57] were proposed to extract either the Mellin moments or x-dependent PDFs by expanding in z^2 . Several other approaches [58–64] also became available in the past few years.

Soon after the theoretical breakthrough, significant progress has been made for the calculation of PDFs [57,65–98], including higher-twist distributions [99–102], parton distribution amplitudes [103–110], GPDs [111–120] as well as transverse-momentum dependent parton distributions [121–126]. More information can be found in several recent reviews [55,127–130].

For GPDs in particular, the Dirac structure $\gamma^{\mu} = \gamma^0$ was usually taken for the quasi-GPD matrix elements as proposed for quasi-PDFs and inspired by the γ^+ definition in the light cone. This definition is, however, frame-dependent for GPDs, requiring that calculations are defined in the symmetric kinematic frame: the momentum transfer is symmetrically distributed as $\vec{p}_f = \vec{P} + \vec{\Delta}/2$ and $\vec{p}_i = \vec{P} - \vec{\Delta}/2$. Encouraging results were reported, with, however, a heavy computational cost for every value of the momentum transfer [111–117].

It was recently proposed and numerically proven that one can equivalently relate the matrix elements in any kinematic frame (e.g., $\vec{p}_f = \vec{P}$ and $\vec{p}_i = \vec{P} - \vec{\Delta})$ to the symmetric one, through Lorentz-invariant amplitudes based on the Lorentz-covariant parameterization of the matrix elements [118–120.131]. This finding established a basis for faster and more efficient computation of GPDs using lattice QCD in asymmetric frames, allowing for flexibility in the distribution of transferred momentum between the initial and final states. Additionally, a novel Lorentz-invariant definition of quasi-GPDs matrix elements was proposed in the same work, which may lead to smaller power corrections in matching to the light-cone GPDs. Based on that, exploratory results using x-space matching and RI-MOM renormalization were established. In this work, we instead will apply the leading-twist short-distance factorization in coordinate space with a ratio-scheme renormalization to extract the first moments of GPDs at a broad range of values for the momentum transfer. By comparing our results with traditional moment calculations, we will be able to assess the efficacy of different definitions for quasi-GPDs, as well as access higher-order moments that are difficult or even impossible to calculate through traditional methods.

The plan of the paper is as follows. In Sec. II, we review the definition of quasi *H* and *E* GPDs. In Sec. III, we present our bare quasi-GPD matrix elements and the ratio scheme renormalization. In Sec. IV, we discuss the determination of Mellin moments of the proton GPDs using short-distance factorization with perturbative matching. In Sec. V, we discuss the *t*-dependence of GPD moments to determine the quark charges, momentum fraction, and total spin contribution to the proton. Additionally, we provide an interpretation of the results in the impact parameter space. Finally, Sec. VI contains our conclusions. Some supplementary material is presented in the Appendix.

¹Alternatively, $P = (p_f + p_i)/2$, $\Delta = p_f - p_i$.

II. QUASI H AND E GPD MATRIX ELEMENTS

As discussed in Ref. [118], the quasi-GPD matrix elements can be parametrized in terms of Lorentz-invariant amplitudes A_i , with certain kinematic factors. Therefore, quasi-GPD matrix elements in different frames can be related to each other, which largely reduces the computational cost for the study of GPDs at various values for the momentum transfer. This can be achieved via a calculation in a convenient asymmetric frame, in which the initial or final states do not carry any momentum transfer. Here, we choose $\vec{p}_f = \vec{P}$ and $\vec{p}_i = \vec{P} - \vec{\Delta}$. In this section, we will review some of the key aspects of Ref. [118], on which this work relies.

For spin-1/2 particles like the proton, the matrix elements defined in Eq. (1) can be parametrized in terms of eight linearly-independent Dirac structures multiplied by eight Lorentz-invariant (frame-independent) amplitudes,

$$F^{\mu}(z, P, \Delta)$$

$$= \bar{u}(p_f, \lambda') \left[\frac{P^{\mu}}{m} \mathcal{A}_1 + mz^{\mu} \mathcal{A}_2 + \frac{\Delta^{\mu}}{m} \mathcal{A}_3 + im\sigma^{\mu z} \mathcal{A}_4 \right]$$

$$+ \frac{i\sigma^{\mu\Delta}}{m} \mathcal{A}_5 + \frac{P^{\mu}i\sigma^{z\Delta}}{m} \mathcal{A}_6 + mz^{\mu}i\sigma^{z\Delta} \mathcal{A}_7$$

$$+ \frac{\Delta^{\mu}i\sigma^{z\Delta}}{m} \mathcal{A}_8 \left[u(p_i, \lambda), \right]$$
(2)

where $\sigma^{\mu\nu} \equiv \frac{i}{2} (\gamma^{\mu} \gamma^{\nu} - \gamma^{\nu} \gamma^{\mu})$, $\sigma^{\mu z} \equiv \sigma^{\mu\rho} z_{\rho}$, $\sigma^{\mu \Delta} \equiv \sigma^{\mu\rho} \Delta_{\rho}$, $\sigma^{z\Delta} \equiv \sigma^{\rho\tau} z_{\rho} \Delta_{\tau}$, $A_i \equiv A_i (z \cdot P, z \cdot \Delta, \Delta^2, z^2)$. For convenience, we use the compact notation $A_i \equiv A_i (z \cdot P, z \cdot \Delta, \Delta^2, z^2)$. For the case of unpolarized quarks, there are two (vector) light-cone GPDs H and E defined through [6],

$$F^{+}(z, P, \Delta) = \bar{u}(p_f, \lambda') \left[\gamma^{+} H(z, P, \Delta) + \frac{i\sigma^{+\mu}\Delta_{\mu}}{2m} E(z, P, \Delta) \right] u(p_i, \lambda).$$
(3)

Combining Eqs. (2) and (3), one can derive,

$$H(z, P, \Delta) = \mathcal{A}_1 + \frac{\Delta^+}{P^+} \mathcal{A}_3, \tag{4}$$

$$E(z, P, \Delta) = -A_1 - \frac{\Delta^+}{P^+} A_3 + 2A_5 + 2P^+ z^- A_6 + 2\Delta^+ z^- A_8,$$
 (5)

where $z^2 = 0$ is always ensured, since $z = ln_{-}$ is along the light-cone direction. Meanwhile, it is worth noting that the light-cone GPDs are solely dependent on Lorentz scalars, rendering them frame-independent.

A similar approached can be followed in a Euclidean lattice calculation. Thus, historically, the quasi-GPD are defined from the $\gamma^{\mu} = \gamma^{0}$ matrix elements with spatial separation $z = (0, 0, 0, z_{3})$, inspired by the success of quasi-PDFs and the lack of finite mixing [132],

$$F^{0}(z, P, \Delta)$$

$$= \langle p_{f}, \lambda' | \bar{q} \left(-\frac{z}{2} \right) \gamma^{0} q \left(\frac{z}{2} \right) | p_{i}, \lambda \rangle$$

$$= \bar{u}(p_{f}, \lambda') \left[\gamma^{0} \mathcal{H}_{0}(z, P, \Delta) + \frac{i \sigma^{0\mu} \Delta_{\mu}}{2m} \mathcal{E}_{0}(z, P, \Delta) \right] u(p_{i}, \lambda).$$
(6)

We can again express them in terms of the Lorentz-invariant amplitudes, A_i . For example, in the symmetric frame with $\vec{p}_f = \vec{P}^s + \vec{\Delta}^s/2$ and $\vec{p}_i = \vec{P}^s - \vec{\Delta}^s/2$, one obtains

$$\mathcal{H}_{0}^{s}(z, P^{s}, \Delta^{s}) = \mathcal{A}_{1} + \frac{\Delta^{0,s}}{P^{0,s}} \mathcal{A}_{3} - \frac{m^{2} \Delta^{0,s} z^{3}}{2P^{0,s} P^{3,s}} \mathcal{A}_{4} + \left[\frac{(\Delta^{0,s})^{2} z^{3}}{2P^{3,s}} - \frac{\Delta^{0,s} \Delta^{3,s} z^{3} P^{0,s}}{2(P^{3,s})^{2}} - \frac{z^{3} (\Delta^{s}_{\perp})^{2}}{2P^{3,s}} \right] \mathcal{A}_{6}$$

$$+ \left[\frac{(\Delta^{0,s})^{3} z^{3}}{2P^{0,s} P^{3,s}} - \frac{(\Delta^{0,s})^{2} \Delta^{3,s} z^{3}}{2(P^{3,s})^{2}} - \frac{\Delta^{0,s} z^{3} (\Delta^{s}_{\perp})^{2}}{2P^{0,s} P^{3,s}} \right] \mathcal{A}_{8},$$

$$(7)$$

$$\mathcal{E}_{0}^{s}(z, P^{s}, \Delta^{s}) = -\mathcal{A}_{1} - \frac{\Delta^{0,s}}{P^{0,s}} \mathcal{A}_{3} + \frac{m^{2} \Delta^{0,s} z^{3}}{2P^{0,s} P^{3,s}} \mathcal{A}_{4} + 2\mathcal{A}_{5} + \left[-\frac{(\Delta^{0,s})^{2} z^{3}}{2P^{3,s}} + \frac{P^{0,s} \Delta^{0,s} \Delta^{3,s} z^{3}}{2(P^{3,s})^{2}} + \frac{z^{3} (\Delta_{\perp}^{s})^{2}}{2P^{3,s}} - \frac{2z^{3} (P^{0,s})^{2}}{P^{3,s}} \right] \mathcal{A}_{6} + \left[-\frac{(\Delta^{0,s})^{3} z^{3}}{2P^{0,s} P^{3,s}} + \frac{(\Delta^{0,s})^{2} \Delta^{3,s} z^{3}}{2(P^{3,s})^{2}} + \frac{\Delta^{0,s} z^{3} (\Delta_{\perp}^{s})^{2}}{2P^{0,s} P^{3,s}} - \frac{2z^{3} P^{0,s} \Delta^{0,s}}{P^{3,s}} \right] \mathcal{A}_{8}.$$

$$(8)$$

while for the asymmetric frame with $\vec{p}_f = \vec{P}^a$ and $\vec{p}_i = \vec{P}^a - \vec{\Delta}^a$, the quasi-GPDs read

$$\mathcal{H}_{0}^{a}(z, P^{a}, \Delta^{a}) = \mathcal{A}_{1} + \frac{\Delta^{0,a}}{P^{0,a}} \mathcal{A}_{3} - \left[\frac{m^{2} \Delta^{0,a} z^{3}}{2P^{0,a} P^{3,a}} - \frac{1}{\left(1 + \frac{\Delta^{3,a}}{2P^{3,a}}\right)} \frac{m^{2} \Delta^{0,a} \Delta^{3,a} z^{3}}{4P^{0,a} (P^{3,a})^{2}} \right] \mathcal{A}_{4}$$

$$+ \left[\frac{(\Delta^{0,a})^{2} z^{3}}{2P^{3,a}} - \frac{1}{\left(1 + \frac{\Delta^{3,a}}{2P^{3,a}}\right)} \frac{(\Delta^{0,a})^{2} \Delta^{3,a} z^{3}}{4(P^{3,a})^{2}} - \frac{1}{\left(1 + \frac{\Delta^{3,a}}{2P^{3,a}}\right)} \frac{P^{0,a} \Delta^{0,a} \Delta^{3,a} z^{3}}{2(P^{3,a})^{2}} - \frac{z^{3} (\Delta^{a}_{\perp})^{2}}{2P^{3,a}} \right] \mathcal{A}_{6}$$

$$+ \left[\frac{(\Delta^{0,a})^{3} z^{3}}{2P^{0,a} P^{3,a}} - \frac{1}{\left(1 + \frac{\Delta^{3,a}}{2P^{3,a}}\right)} \frac{(\Delta^{0,a})^{3} \Delta^{3,a} z^{3}}{4P^{0,a} (P^{3,a})^{2}} - \frac{1}{\left(1 + \frac{\Delta^{3,a}}{2P^{3,a}}\right)} \frac{(\Delta^{0,a})^{2} \Delta^{3,a} z^{3}}{2(P^{3,a})^{2}} - \frac{z^{3} (\Delta^{a}_{\perp})^{2} \Delta^{0,a}}{2P^{0,a} P^{3,a}} \right] \mathcal{A}_{8}, \quad (9)$$

$$\mathcal{E}_{0}^{a}(z, P^{a}, \Delta^{a}) = -\mathcal{A}_{1} - \frac{\Delta^{0,a}}{P^{0,a}} \mathcal{A}_{3} - \left[-\frac{m^{2}\Delta^{0,a}z^{3}}{2P^{0,a}P^{3,a}} - \frac{1}{\left(1 + \frac{\Delta^{3,a}}{2P^{3,a}}\right)} \left(\frac{m^{2}z^{3}}{P^{3,a}} - \frac{m^{2}\Delta^{0,a}\Delta^{3,a}z^{3}}{4P^{0,a}(P^{3,a})^{2}} \right) \right] \mathcal{A}_{4} + 2\mathcal{A}_{5}$$

$$+ \left[-\frac{(\Delta^{0,a})^{2}z^{3}}{2P^{3,a}} - \frac{1}{\left(1 + \frac{\Delta^{3,a}}{2P^{3,a}}\right)} \left(\frac{P^{0,a}\Delta^{0,a}z^{3}}{P^{3,a}} - \frac{(\Delta^{0,a})^{2}\Delta^{3,a}z^{3}}{4(P^{3,a})^{2}} \right) - \frac{1}{\left(1 + \frac{\Delta^{3,a}}{2P^{3,a}}\right)} \left(\frac{2z^{3}(P^{0,a})^{2}}{P^{3,a}} - \frac{P^{0,a}\Delta^{0,a}\Delta^{3,a}z^{3}}{2(P^{3,a})^{2}} \right) + \frac{z^{3}(\Delta^{a}_{\perp})^{2}}{2P^{3,a}} \right] \mathcal{A}_{6} + \left[-\frac{(\Delta^{0,a})^{3}z^{3}}{2P^{0,a}P^{3,a}} - \frac{1}{\left(1 + \frac{\Delta^{3,a}}{2P^{3,a}}\right)} \left(\frac{(\Delta^{0,a})^{2}z^{3}}{P^{3,a}} - \frac{(\Delta^{0,a})^{3}\Delta^{3,a}z^{3}}{4P^{0,a}(P^{3,a})^{2}} \right) - \frac{1}{\left(1 + \frac{\Delta^{3,a}}{2P^{3,a}}\right)} \left(\frac{2z^{3}P^{0,a}\Delta^{0,a}}{P^{3,a}} - \frac{(\Delta^{0,a})^{2}\Delta^{3,a}z^{3}}{2(P^{3,a})^{2}} \right) + \frac{z^{3}(\Delta^{a}_{\perp})^{2}\Delta^{0,a}}{2P^{0,a}P^{3,a}} \right] \mathcal{A}_{8}.$$

$$(10)$$

It is evident that when the hadron momentum $\vec{P} = (0,0,P_3)$ is finite, the definition of γ^0 varies across different frames, though such discrepancies vanish in the infinite momentum limit. What follows is the question of which definition could be an appropriate choice that can provide good convergence to the light-cone quantities, and can be described by the perturbative matching. To explore this possibility, inspired by Eqs. (4) and (5), it is natural to define the quasi-GPD matrix elements also in a Lorentz-invariant form as

$$\mathcal{H}_{LI}^{s/a}(z \cdot P, z \cdot \Delta, (\Delta)^2, z^2) = \mathcal{A}_1 + \frac{\Delta \cdot z}{P \cdot z} \mathcal{A}_3, \quad (11)$$

$$\mathcal{E}_{LI}^{s/a}(z \cdot P, z \cdot \Delta, (\Delta)^{2}, z^{2})
= -\mathcal{A}_{1} - \frac{\Delta \cdot z}{P \cdot z} \mathcal{A}_{3} + 2\mathcal{A}_{5} + 2P \cdot z\mathcal{A}_{6} + 2\Delta \cdot z\mathcal{A}_{8}, \quad (12)$$

with the only difference with their light-cone counterpart H and E being $z^2 \neq 0$ originated from the spatial separation such as $z = (0,0,0,z_3)$. All the amplitudes $\mathcal{A}_i^{s/a}$ can be extracted from either the symmetric or an asymmetric frame through linear combinations of the various F^{μ} ($\mu = 0, 1, 2, 3$), and any choice can be used in Eqs. (7)–(12) as long as a Lorentz transformation is applied to the kinematic factors to match the values of t.

Consequentially, we can construct the quasi-GPDs in any frame, including the Lorentz-invariant ones, as has been proven in Ref. [118]. In addition, with a reduced number of additional terms, the proposed Lorentz-invariant definition could potentially converge to the light-cone GPDs faster than the γ^0 definition. To explore this possibility, we will analyze results from different definitions and compare them with the traditional Mellin-moments calculations in this work.

III. BARE MATRIX ELEMENTS AND RATIO SCHEME RENORMALIZATION

A. Lattice setup

In this study, we use a gauge ensemble of $N_f=2+1+1$ twisted-mass fermions with a clover term and Iwasaki-improved gluons [133]. The lattice size and spacing of the ensemble are $N_s \times N_t = 32^3 \times 64$ and a=0.093 fm, respectively. The quark masses are tuned to produce a pion mass of 260 MeV. To extract the bare matrix elements of quasi-GPDs, we need to compute the two-point and three-point functions, namely

$$C^{2\text{pt}}(\Gamma_0, p; t_s) = \sum_{\vec{y}} e^{-i\vec{p}\cdot(\vec{y}-\vec{x})} \Gamma^0_{\alpha\beta} \langle N^{(s)}_{\alpha}(\vec{y}, t_s) \bar{N}^{(s')}_{\beta}(\vec{x}, 0) \rangle,$$

$$(13)$$

and,

$$C^{\text{3pt}}_{\mu}(\Gamma_{\kappa}, p_f, p_i; t_s, \tau) = \sum_{\vec{y}, \vec{z}_0} e^{-i\vec{p}_f \cdot (\vec{y} - \vec{x})} e^{-i\vec{q} \cdot (\vec{x} - \vec{z}_0)} \Gamma^{\kappa}_{\alpha\beta} \langle N_{\alpha}(\vec{y}, t_s) \mathcal{O}_{\mu}(\vec{z}_0 + z\hat{z}, \tau) \bar{N}_{\beta}(\vec{x}, 0) \rangle, \tag{14}$$

where $N^{(s)}$ is the standard nucleon source under momentum smearing [134] to improve the overlap with the proton ground state and suppress gauge noise. It was found that the statistical noise is z-dependent and reduces by a factor of 4–5 in the real part, and 2–3 in the imaginary part of the unpolarized GPDs [112]. $\mathcal{O}_{\mu} = \bar{\psi}(z)\gamma_{\mu}\mathcal{W}(0,z)\psi(0)$ is the equal-time nonlocal operator with the quark fields separated along the z direction. In this work, we compute the isovector (u-d) and isoscalar (u+d) flavor combination. For the isoscalar case, we ignore the disconnected diagrams, which were found to be negligible for the unpolarized case [92]. The unpolarized and polarized parity projectors Γ_0 and Γ_{κ} are defined as

$$\Gamma_0 = \frac{1}{4}(1 + \gamma_0),\tag{15}$$

$$\Gamma_{\kappa} = \frac{1}{4} (1 + \gamma_0) i \gamma_5 \gamma_{\kappa}, \qquad \kappa = 1, 2, 3.$$

$$\tag{16}$$

Taking advantage of the correlations between two- and three-point functions, we construct the ratio,

$$R_{\kappa}^{\mu}(\Gamma_{\kappa}, p_{f}, p_{i}; t_{s}, \tau) = \frac{C_{\mu}^{3\text{pt}}(\Gamma_{\kappa}, p_{f}, p_{i}; t_{s}, \tau)}{C^{2\text{pt}}(\Gamma_{0}, p_{f}; t_{s})} \sqrt{\frac{C^{2\text{pt}}(\Gamma_{0}, p_{i}, t_{s} - \tau)C^{2\text{pt}}(\Gamma_{0}, p_{f}, \tau)C^{2\text{pt}}(\Gamma_{0}, p_{f}, t_{s})}{C^{2\text{pt}}(\Gamma_{0}, p_{f}; t_{s})}},$$
(17)

which, in the $t_s \to \infty$ limit, corresponds to the bare matrix elements of proton ground state matrix elements $\lim_{t_s \to \infty} R_\kappa^\mu = \Pi_\mu(\Gamma_\kappa)$. To keep the statistical noise under control, we use a source-sink separation of $t_s = 10a = 0.93$ fm and take a plateau fit with respect to τ in a region of convergence. We postpone the study of excited states for future work targeting precision control. In Table I, we show the momenta $\vec{P} = (0,0,P_3)$ and $\vec{\Delta}$ as well as the statistics used in this work, where the notation for the symmetric frame is,

$$\vec{p}_{f}^{s} = \vec{P} + \frac{\vec{\Delta}}{2} = \left(+\frac{\Delta_{1}}{2}, +\frac{\Delta_{2}}{2}, P_{3} \right),$$

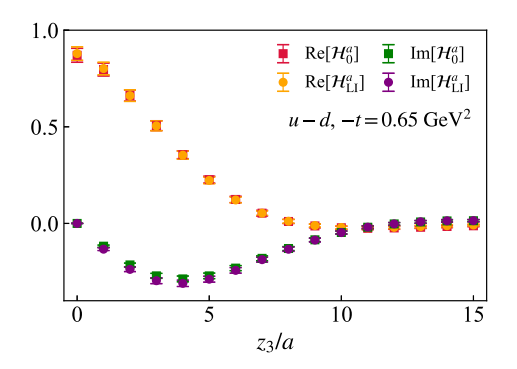
$$\vec{p}_{i}^{s} = \vec{P} - \frac{\vec{\Delta}}{2} = \left(-\frac{\Delta_{1}}{2}, -\frac{\Delta_{2}}{2}, P_{3} \right),$$
(18)

and for the asymmetric frame, in which all the momentum transfer is assigned to the initial state, is

$$\vec{p}_f^a = \vec{P} = (0, 0, P_3), \quad \vec{p}_i^a = \vec{P} - \vec{\Delta} = (-\Delta_1, -\Delta_2, P_3).$$
 (19)

TABLE I. Statistics for the symmetric and asymmetric frame matrix elements are shown. N_{ME} , N_{confs} , N_{src} and N_{total} are the number of matrix elements, configurations, source positions per configuration and total statistics, respectively.

Frame	P_3 [GeV]	$\mathbf{\Delta} \left[\frac{2\pi}{L} \right]$	-t [GeV ²]	ξ	$N_{ m ME}$	$N_{\rm confs}$	$N_{\rm src}$	$N_{\rm tot}$
N/A	±1.25	(0, 0, 0)	0	0	2	329	16	10528
Symmetric	± 0.83	$(\pm 2, 0, 0), (0, \pm 2, 0)$	0.69	0	8	67	8	4288
Symmetric	± 1.25	$(\pm 2, 0, 0), (0, \pm 2, 0)$	0.69	0	8	249	8	15936
Symmetric	± 1.67	$(\pm 2, 0, 0), (0, \pm 2, 0)$	0.69	0	8	294	32	75264
Symmetric	± 1.25	$(\pm 2, \pm 2, 0)$	1.38	0	16	224	8	28672
Symmetric	± 1.25	$(\pm 4, 0, 0), (0, \pm 4, 0)$	2.77	0	8	329	32	84224
Asymmetric	± 1.25	$(\pm 1, 0, 0), (0, \pm 1, 0)$	0.17	0	8	269	8	17216
Asymmetric	± 1.25	$(\pm 1, \pm 1, 0)$	0.34	0	16	195	8	24960
Asymmetric	± 1.25	$(\pm 2, 0, 0), (0, \pm 2, 0)$	0.65	0	8	269	8	17216
Asymmetric	± 1.25	$(\pm 1, \pm 2, 0), (\pm 2, \pm 1, 0)$	0.81	0	16	195	8	24960
Asymmetric	± 1.25	$(\pm 2, \pm 2, 0)$	1.24	0	16	195	8	24960
Asymmetric	± 1.25	$(\pm 3, 0, 0), (0, \pm 3, 0)$	1.38	0	8	269	8	17216
Asymmetric	± 1.25	$(\pm 1, \pm 3, 0), (\pm 3, \pm 1, 0)$	1.52	0	16	195	8	24960
Asymmetric	±1.25	$(\pm 4, 0, 0), (0, \pm 4, 0)$	2.29	0	8	269	8	17216



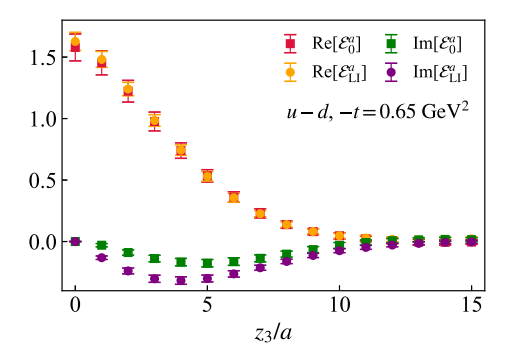


FIG. 1. Bare matrix elements of the isovector quasi-GPDs from the asymmetric frame with momentum transfer -t = 0.65 GeV². The left panel shows \mathcal{H}_0^a from the γ_0 definition and \mathcal{H}_{LI}^a from the Lorentz-invariant definition, while the right panel shows \mathcal{E}_0^a from the γ_0 definition and \mathcal{E}_{LI}^a from the Lorentz-invariant definition.

While \vec{P} and $\vec{\Delta}$ are the same for both frames, they lead to different values of -t due to the different distribution of the momentum transfer, that is

$$-t^s = \vec{\Delta}^2$$
, $-t^a = \vec{\Delta}^2 - (E(p') - E(p))^2$. (20)

We note that this work focuses on zero skewness, namely $\Delta_3 = 0$, and most of the hadron momentum P is fixed at 1.25 GeV throughout the calculation. We combine all data contributing to the same value of momentum transfer $t = -\Delta^2$ with definite symmetry with respect to $P_3 \rightarrow -P_3$, $z_3 \rightarrow -z_3$, and $\vec{\Delta} \rightarrow -\vec{\Delta}$.

In Fig. 1, we compare the isovector bare matrix elements under the γ^0 definition with the Lorentz-invariant definition, as extracted from the asymmetric frame data with momentum transfer $-t=0.65~{\rm GeV^2}$. As one can see, the difference between the two definitions for the ${\cal H}$ GPD is almost negligible, whereas, for the ${\cal E}$ GPD, particularly its imaginary part, the difference is considerable. This effect is similarly observed at other values of momentum transfer and will be reflected in the moments obtained through the subsequent analysis. In Fig. 2, we summarize all the matrix elements at various values of -t using the Lorentz-invariant definition derived from amplitudes ${\cal A}_i^{s/a}$ in both asymmetric and symmetric frames. The matrix elements under the γ_0

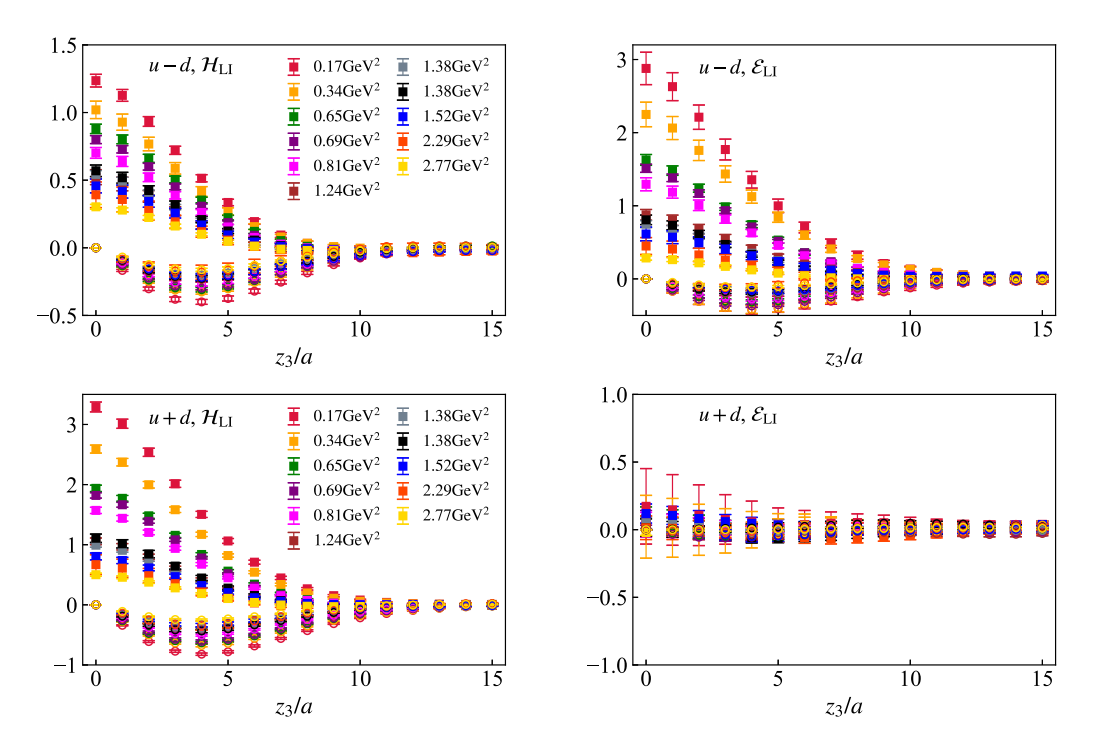


FIG. 2. Bare matrix elements under Lorentz-invariant definition constructed from amplitudes $A_i^{s/a}$ from both asymmetric and symmetric frame. The upper and lower panels are for the isovector and isoscalar cases, with squared points for the real part and circled points for the imaginary part. The data shown are from hadron momentum $P_3 = 1.25$ GeV with all values of -t indicated in Table I.

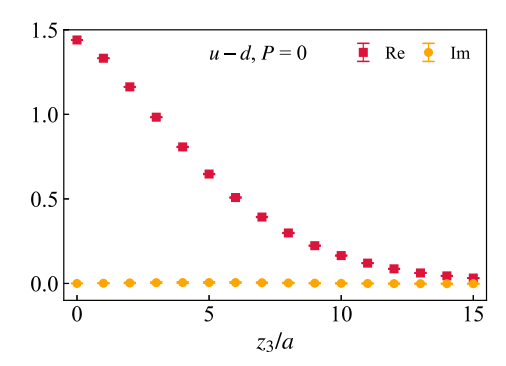


FIG. 3. Bare matrix elements of isovector zero-momentum quasi-PDF matrix elements $\mathcal{F}(z, P=0, \Delta=0)$.

definition are shown in Appendix C. We clarify that \mathcal{H}_0^s and \mathcal{E}_0^s use \mathcal{A}_i^s , while \mathcal{H}_0^a and \mathcal{E}_0^a use \mathcal{A}_i^a . We remind the reader that one may use the \mathcal{A}_i from any frame along with the appropriate Lorentz transformation to the kinematic coefficients. The isovector and isoscalar cases are both shown in the upper and lower panels, with squared points for the real part and circled points for the imaginary part. As one can observe, the matrix elements exhibit a decreasing trend as the momentum transfer -t increases. In the isoscalar case, the \mathcal{E}_{LI} are mostly consistent with zero within the errors. For completeness, we show in Fig. 3 the bare matrix element for the isovector quasi-PDF that is used in the ratio renormalization scheme, which are purely real.

B. Ratio scheme renormalization

The bare matrix elements contain UV divergences related to the operator and the Wilson line. Thus, we have to renormalize the matrix elements prior to extracting physical quantities. It is known that the UV divergence of the quark bilinear operator is multiplicative and independent of the Dirac structure Γ_{μ} matrix as well as the hadron state [135–137]. One can therefore remove the UV divergence by constructing the renormalization group (RG) invariant ratios using the bare matrix elements with different hadron states but the same operators [88]. In this work, we construct the ratios,

$$\mathcal{M}(z, P, \Delta) = \frac{\mathcal{F}(\vec{z}, \vec{P}, \vec{\Delta})}{\mathcal{F}(\vec{z}, \vec{P} = 0, \vec{\Delta} = 0)}$$
$$= \frac{\mathcal{F}^{R}(\vec{z}, \vec{P}, \vec{\Delta})}{\mathcal{F}^{R}(\vec{z}, \vec{P} = 0, \vec{\Delta} = 0)}, \tag{21}$$

where the ratio of bare matrix elements \mathcal{F} is RG invariant, so that is equivalent to the ratio of renormalized matrix elements \mathcal{F}^R . $\mathcal{F}(\vec{z}, \vec{P}, \vec{\Delta})$ in the numerator can be either \mathcal{H} or \mathcal{E} quasi-GPDs for the isovector (u-d) and isoscalar (u+d) cases. For the denominator, we chose to always take the isovector $\vec{P}=0$ quasi-PDF matrix elements as shown in Fig. 3, since the renormalization factors are

identical. A discussion of isoscalar $\vec{P}=0$ quasi-PDF matrix elements can be found in Appendix B. At z=0, the isovector matrix element $\mathcal{F}(\vec{z}=0,\vec{P}=0,\vec{\Delta}=0)$ gives the renormalization constant Z_V .

The RG invariant ratios, $\mathcal{M}(z, P, \Delta)$, can also be written as a function of Lorentz-invariant variables, that is, $\mathcal{M}(z^2, zP, \Delta^2)$, with the $zP = z_3P_3$ being the so-called Infection Infection Infection Infection zP instead of z_3P_3 in what follows. If the momentum transfer Δ equals zero in \mathcal{F} , the $\mathcal{M}(z, P, \Delta = 0)$ will reduce to the standard Ioffe-time pseudo-distribution [56,57]. In Fig. 4, we show the ratio scheme renormalized matrix elements for the isovector (upper panels) and isoscalar (lower panels) quasi-GPDs. The matrix elements shown are from the Lorentz-invariant definition of quasi-GPDs (bare matrix elements presented in Fig. 2, with the filled squared symbols for the real part and the circled open symbols for the imaginary part. It can be seen that the renormalized matrix elements have a good signal and show a clear dependence on the momentum transfer -t. The isoscalar \mathcal{E} quasi-GPDs are still mostly consistent with zero after renormalization, as also observed in the bare case.

IV. SHORT DISTANCE FACTORIZATION AND MELLIN MOMENTS

A. Short distance factorization

The renormalized matrix elements can be expanded in z^2 , namely the short distance factorization (SDF). In the case of zero skewness, $\xi = 0$, the leading-twist SDF for the quasi-GPDs is the same as in the quasi-PDF case [138], which in the $\overline{\rm MS}$ scheme reads [56,57,139],

$$\mathcal{F}^{\overline{\mathrm{MS}}}(z, P, \Delta) = \sum_{n=0} \frac{(-izP)^n}{n!} C_n^{\overline{\mathrm{MS}}}(\mu^2 z^2) \langle x^n \rangle + \mathcal{O}(\Lambda_{\mathrm{QCD}}^2 z^2),$$
(22)

where $C_n^{\overline{\rm MS}}(\mu^2 z^2)$ are Wilson coefficients calculated from perturbation theory, which are available up to NNLO [140,141] for the isovector (u-d) case, but only up to NLO for the isoscalar (u+d) one with complete calculation including the quark-gluon mixing [142]. The $\langle x^n \rangle$ are the Mellin moments of GPDs, defined as

$$\int_{-1}^{1} dx x^{n} H^{q}(x, \xi = 0, t) = \sum_{\substack{i=0 \text{even}}}^{n} A_{n+1,i}^{q}(t),$$

$$\int_{-1}^{1} dx x^{n} E^{q}(x, \xi = 0, t) = \sum_{\substack{i=0 \text{even}}}^{n} B_{n+1,i}^{q}(t), \tag{23}$$

in which the second moments $\langle x \rangle$, namely A_{20} and B_{20} , are of particular interest due to their connection to the QCD energy-momentum tensor as gravitational form factors and

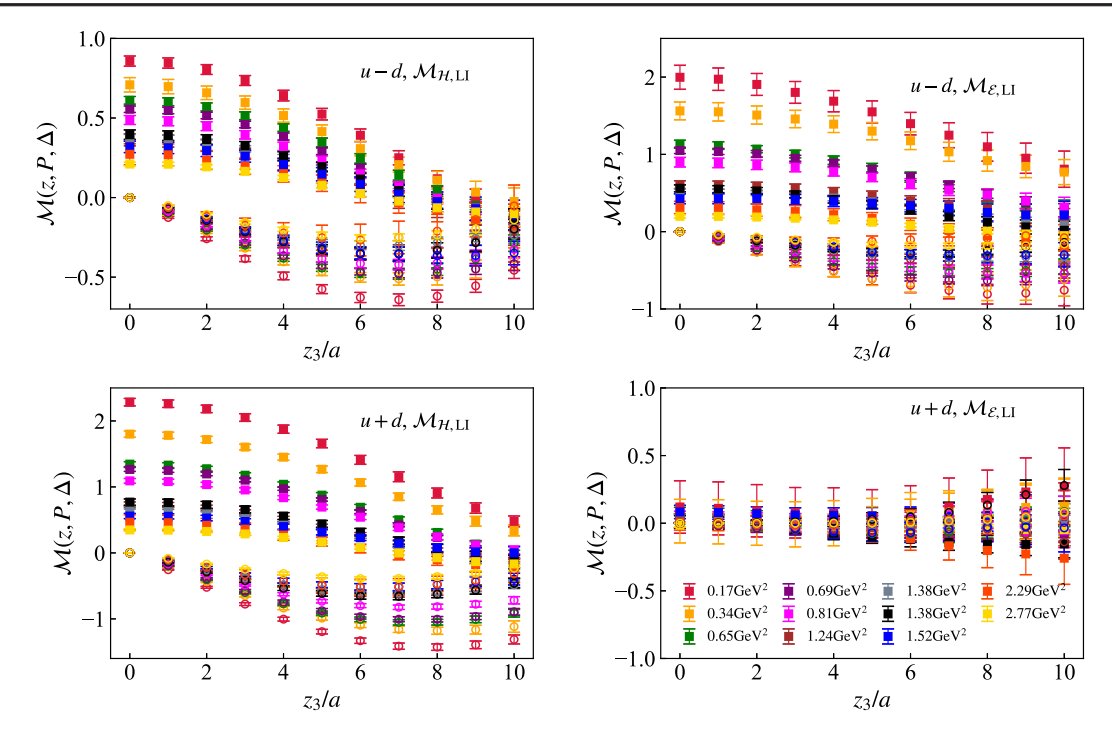


FIG. 4. Ratio scheme renormalized matrix elements $\mathcal{M}(z, P_z, P_z^0)$ for isovector (u-d) case (upper panels) and isoscalar (u+d) case (lower panels). The filled squared symbols are for the real part, while the circled open symbols are for the imaginary part.

provide access to the angular momentum sum rule. The $\langle x^0 \rangle$ are essentially the Dirac (for H) and Pauli (for E) form factors. This SDF formula suffers from higher-twist contamination $\mathcal{O}(\Lambda_{\rm OCD}^2 z^2)$ growing as a function of z^2 . Thus, it is expected to be valid for small spatial separations z^2 . As a consequence, the matrix elements will only be sensitive to the lower moments, as the higher ones are factorially suppressed by $(-izP)^n/n!$ for a finite hadron momentum P_3 . Despite the abovementioned challenges, it is desirable to pursue the direction of extracting Mellin moments from an SDF, because traditional calculations of higherorder moments through local operators suffer from notorious mixing between higher-dimensional and lowerdimensional operators [33–51]. In contrast, quasi-GPDs involve only a nonlocal operator of dimension three, and therefore, the higher moments can be systematically accessed by increasing the hadron momentum. Inserting

the SDF formula into the ratio scheme renormalized matrix elements in Sec. III B, one obtains [88,89]

$$\mathcal{M}(z, P, \Delta) = \sum_{n=0} \frac{(-izP)^n}{n!} \frac{C_n^{\overline{\text{MS}}}(\mu^2 z^2)}{C_0^{\overline{\text{MS}}}(\mu^2 z^2)} \langle x^n \rangle + \mathcal{O}(\Lambda_{\text{QCD}}^2 z^2).$$
(24)

The ratio scheme renormalization has the advantage of potentially reducing the higher-twist contamination, because of the latter's cancellation between the numerator and denominator. Nevertheless, it is still important to keep the value of z moderate so that the SDF does not break down. For practical reasons, one needs to truncate Eq. (24) up to $n_{\rm max}$ when performing the fit, and then minimizing the χ^2 defined as,

$$\chi^{2} = \sum_{P_{3}} \sum_{z=z_{\min}}^{z_{\max}} \left(\frac{(\text{Re}[\mathcal{M}^{\text{SDF}}(z, P, \Delta)] - \text{Re}[\mathcal{M}^{\text{data}}(z, P, \Delta)])^{2}}{\sigma_{\text{Re}}^{2}} + \frac{(\text{Im}[\mathcal{M}^{\text{SDF}}(z, P, \Delta)] - \text{Im}[\mathcal{M}^{\text{data}}(z, P, \Delta)])^{2}}{\sigma_{\text{Im}}^{2}} \right), \quad (25)$$

from which we can determine the moments up to $\langle x^{n_{\text{max}}} \rangle$. It is worth mentioning that the real and imaginary parts of $\mathcal{M}(z,P,\Delta)$ will provide even and odd moments, respectively.

B. Fixed- z^2 analysis and pQCD correction

At leading-order approximation, that is, for $\mathcal{O}(\alpha_s^0)$ and with $C_n(\mu^2 z^2) = 1$, the factorization formula in Eq. (24)

reduces to a polynomial function of zP with coefficients $\langle x^n \rangle$ for a fixed momentum transfer -t. Beyond the leading approximation, the renormalized matrix element or the moments nontrivially depend on the physical scale z^2 . At short distance, the Wilson coefficients $C_n(\mu^2 z^2)/C_0(\mu^2 z^2)$ are expected to compensate for this scale dependence and evolve the moments to the factorization scale μ .

At the momentum transfer of $-t = 0.69 \text{ GeV}^2$, we have three different momenta: $P_3 = 0.83$, 1.25 and 1.67 GeV, which can be used to assess the validity of the leading twist factorization. Since the matrix elements of a local current should have no boost or frame dependence at a given -t, we averaged the $z_3 = 0$ matrix elements $\mathcal{M}_{\mathcal{H}}(0, P, \Delta)$ of the three P_3 for each bootstrap sample, and normalized the $\mathcal{M}_{\mathcal{H}}$ by $\mathcal{M}_{\mathcal{H}}(0, P, \Delta)/\overline{\mathcal{M}_{\mathcal{H}}}(0, P, \Delta)$. We also do this for $\mathcal{M}_{\mathcal{E}}$. In the upper panels of Fig. 5, we show the isovector matrix elements $\mathcal{M}_{\mathcal{H},\mathrm{LI}}$ (left panels) and $\mathcal{M}_{\mathcal{E},\mathrm{LI}}$ (right panels) from the Lorentz-invariant definition with momentum transfer $-t = 0.69 \text{ GeV}^2$ as a function of zP, while the ones of the γ_0 definition are shown in the lower panels for comparison. It is evident that, in the case of the Lorentzinvariant definition, the matrix elements for different P_3 values appear to overlap with each other as a function of zP. This observation is consistent with the leading-order approximation of Eq. (24), while the beyond-leading-order effects are only minor, as perturbative contributions fall within the current statistical errors. This finding is also applicable to $\mathcal{M}_{\mathcal{H},\gamma_0}$ under the γ_0 definition. However, when it comes to $\mathcal{M}_{\mathcal{E},\gamma_0}$, the matrix elements from our three momentum values display significant deviations, even at very short distances, especially in the imaginary part. These deviations are more pronounced for smaller momenta, indicating additional power corrections that can be suppressed by P_3 , but remain significant for small momenta. To explore this further, we will extract the moments at each z using the Wilson coefficients at different orders by fitting the P_3 dependence using Eq. (25). We set $n_{\max} = 4$ as the truncation order for the SDF formula, which is expected to be sufficient for the considered momentum range, given the higher-order terms are factorially suppressed, as we will see in the following discussion.

In Fig. 6, we show the first few moments extracted from each fixed z_3/a from isovector $\mathcal{M}_{\mathcal{H},\mathrm{LI}}$ and $\mathcal{M}_{\mathcal{E},\mathrm{LI}}$. We have used the Wilson coefficients from leading order (LO) to next-to-next-to-leading order (NNLO), including the one considering the renormalization group resummation (NNLO + RG) at short distance [96,143]. The factorization scale was set to $\mu=2$ GeV. We leave out the first moments A_{10} and B_{10} , which have no scale dependence as conserved charges. As for the second moments of H and E, A_{20} and B_{20} have the best nonzero signal and exhibit small z-dependence at very short distances in the LO results. What is more, using the NLO, NNLO, and NNLO + RG Wilson coefficients, such z-dependence can be compensated, resulting in plateaus at the factorization scale $\mu=2$ GeV. The differences among NLO, NNLO, and

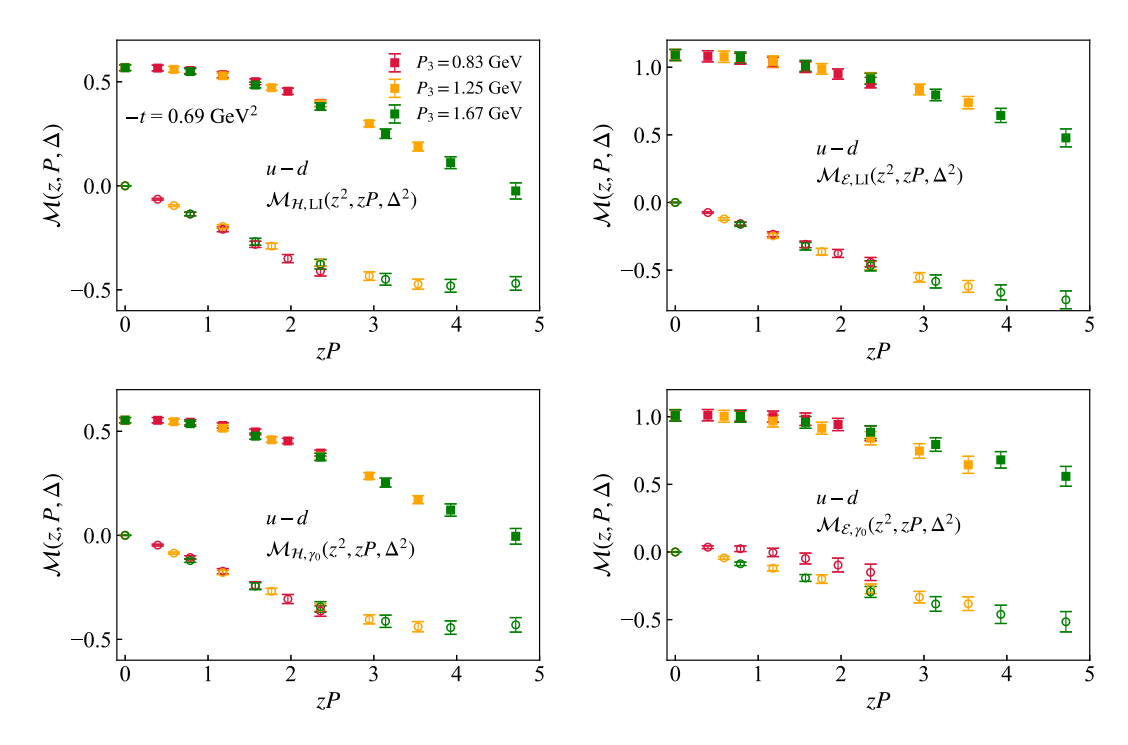


FIG. 5. Isovector ratio scheme renormalized matrix elements from the Lorentz-invariant definition (upper panels) and the γ_0 definition (lower panels) at momentum transfer -t = 0.69 GeV² as a function of zP. The z_3 shown are in the range [a, 6a]. We have three different values of the momentum $P_3 = 0.83$, 1.25 and 1.67 GeV for this -t. The filled squared symbols are for the real part, while the circled open symbols are for the imaginary part.

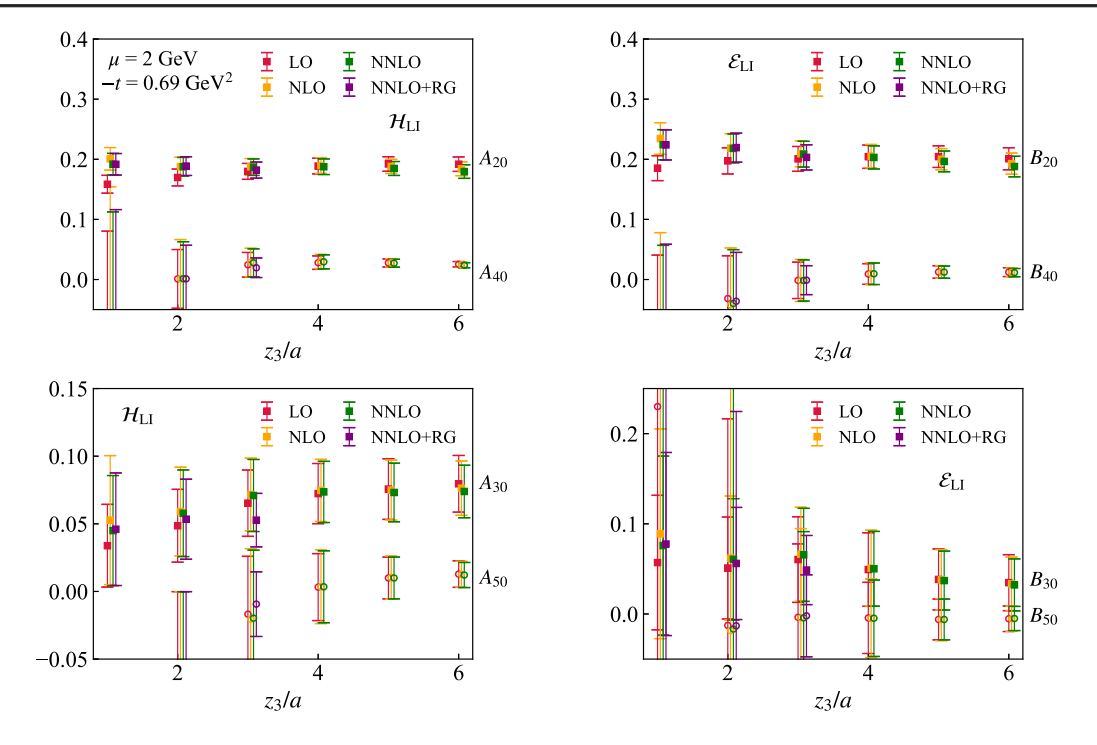


FIG. 6. The left panels show the first few moments extracted at each z from the isovector $\mathcal{M}_{\mathcal{H},\mathrm{LI}}$, while the right panels display the corresponding moments from $\mathcal{M}_{\mathcal{E},\mathrm{LI}}$, for the symmetric case of $P_3 = 0.83$, 1.25, 1.67 GeV and -t = 0.69 GeV², utilizing the data in Fig. 5 and Wilson coefficients at LO, NLO, NNLO, and NNLO + RG order. The filled squared symbols are for the real part, while the circled open symbols are for the imaginary part.

NNLO + RG are compatible with zero within the statistical error. The results with RG are shown only for $z_3 \lesssim 0.3$ fm as $\alpha_s(1/z_3)$ will hit the Landau pole at large z_3 , despite that the fixed-order Wilson coefficients are still finite. In the following analysis, we will use fixed-order Wilson coefficients and vary the range of z_3 to beyond ~0.3 fm to have more data points for estimating the systemics, though a rigorous treatment would require the use of RG improved OPE with only small- z_3 matrix elements. This situation can be improved with finer lattices and larger momenta P_3 in the future.

As for the higher moments that are noisy at short z_3 , no dependence on the perturbative order is observed. These findings are consistent with the fact that the ratio-scheme renormalized matrix elements mostly depend on zP and have very mild dependence on P_3 as observed in Fig. 5, for the Lorentz-invariant definition. For comparison, in Fig. 7 we show the first few moments extracted from $\mathcal{M}_{\mathcal{H},\gamma_0}$ and $\mathcal{M}_{\mathcal{E},\gamma_0}.$ For the moments from $\mathcal{M}_{\mathcal{H},\gamma_0}$ shown in the left panels, similar behavior can be observed as in the case of $\mathcal{M}_{\mathcal{H},II}$, though the central values of moments are slightly shifted. However, strong z_3 dependence can be observed for moments from $\mathcal{M}_{\mathcal{E},\gamma_0}$ as the zP dependence breaks down for the γ_0 definition seen in Fig. 5. It is clear that the perturbative kernels, even up to NNLO, cannot explain this z_3 dependence. We then conclude that the quasi-GPD matrix elements \mathcal{H} and \mathcal{E} under Lorentz-invariant definition, as a function of both z^2 and zP, can be well described by the perturbative kernels together with the ratio-scheme renormalization. However, the factorization formula is not applicable for the quasi-GPD \mathcal{E} with γ_0 definition in the considered range of z_3 and P_3 , because of additional power corrections in this case, as we discussed in Sec. II. A similar observation holds for the isoscalar cases, where we used Wilson coefficients only up to the NLO level and ignored the quark-gluon mixing. Therefore we will use the quasi-GPDs in Lorentz-invariant definition, which may converge to the light-cone GPDs faster, for the following analysis. Meanwhile, we will stick to the best-known Wilson coefficients, NNLO and NLO, for isovector and isoscalar cases, respectively.

C. Determination of Mellin moments

It is found that the perturbative matching can well describe the ratio-scheme renormalized matrix elements under Lorentz-invariant definition. However, the higher moments extracted from fixed z exhibit significant noise. To stabilize the fit, and also because we only have one momentum P_3 for many values of -t, we will perform combined fits of several renormalized matrix elements with $z_3 \in [z_3^{\min}, z_3^{\max}]$. We note that matrix elements at small z may suffer from discretization effects, while at large z they may be affected by higher-twist effects. We omit $z_3 = a$ to avoid the most severe discretization effects and vary

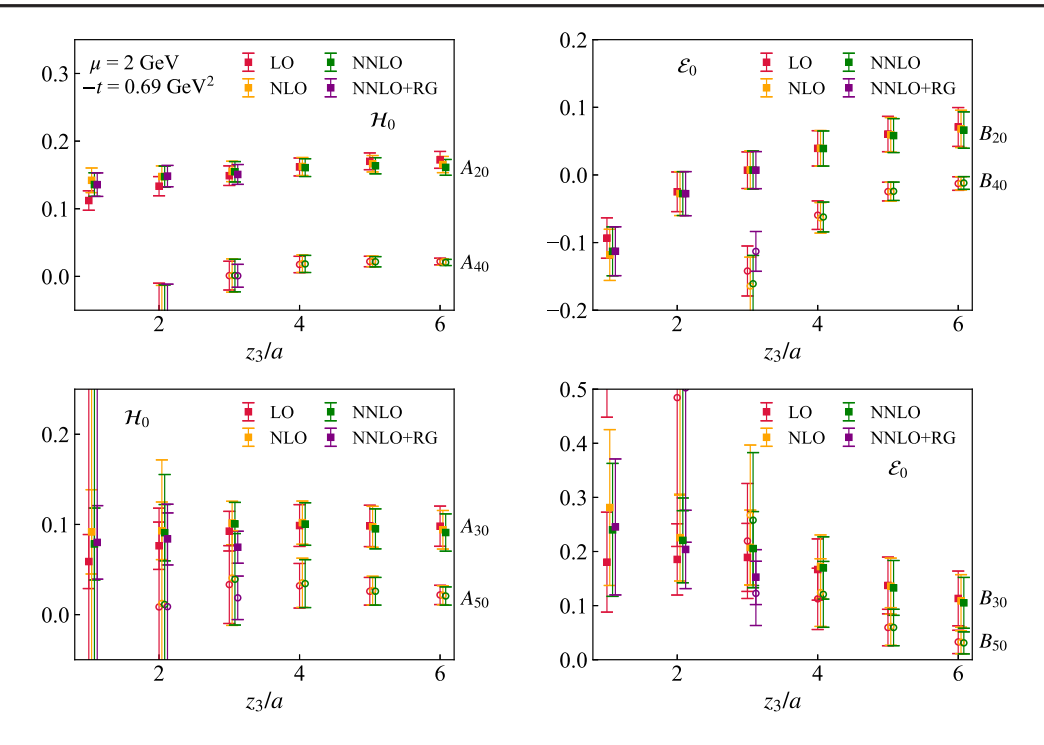
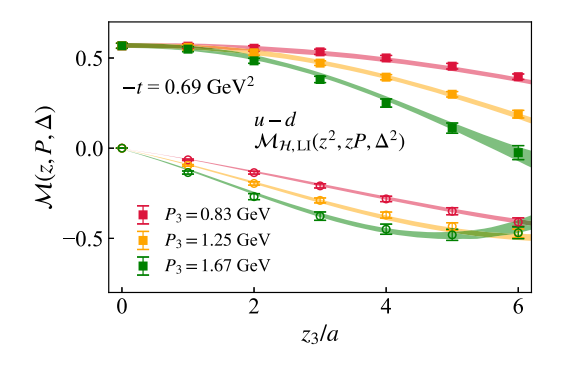


FIG. 7. The left panels show the first few moments extracted at each z from the isovector $\mathcal{M}_{\mathcal{H},\gamma_0}$, while the right panels display the corresponding moments from $\mathcal{M}_{\mathcal{E},\gamma_0}$, for a symmetric case of $P_3=0.83$, 1.25, 1.67 GeV and -t=0.69 GeV², utilizing Wilson coefficients at LO, NLO, NNLO, and NNLO + RG order. The filled squared symbols are for the real part, while the circled open symbols are for the imaginary part.

 $z_3^{\min} \in [2a,3a], \ z_3^{\max} \in [4a,6a]$ to estimate systematic errors related to discretization and higher-twist effects. To be specific, for an observable \mathcal{X} and a given bootstrap sample, we average over the fit results with different $[z_3^{\min}, z_3^{\max}]$ to obtain $\operatorname{Mean}(\mathcal{X})$ and estimate the systematic error as $\operatorname{err}(\mathcal{X}) = \operatorname{Mean}((\mathcal{X} - \operatorname{Mean}(\mathcal{X}))^2)$. Then, we consider all bootstrap samples to obtain the average value of the observable $\overline{\operatorname{Mean}(\mathcal{X})}$ and estimate the statistical uncertainty. The final systematic error is obtained as $\overline{\operatorname{err}(\mathcal{X})}$.

In Fig. 8, we show the fit results from $z_3 \in [2a, 6a]$ at the momentum transfer -t = 0.69 GeV² for $\mathcal{M}_{\mathcal{H}, LI}$ (left panel) and $\mathcal{M}_{\mathcal{E}, LI}$ (right panel) as a function of z_3 . The bands come

from the combined fit with the NNLO kernel, which can describe well the matrix elements. In Fig. 9, we summarize the first five moments of $A_{n+1,0}$ and $B_{n+1,0}$ extracted from $z_3^{\min} = 2a, 3a$ as a function of z_3^{\max} , where reasonable signal can be observed. Meanwhile, the extracted moments show little dependence on z_3^{\min} or z_3^{\max} , suggesting the systematic errors (outer light bands) are small compared to the statistical errors (inner dark bands) at the current stage. It can also be found that the higher moments have smaller values than the lower ones. Together with the fact that they are factorially suppressed by $(-izP)^n/n!$ with finite hadron momentum P_3 , the fourth and fifth moments are still noisy within the $zP\lesssim 5$ used in this work. To further constrain



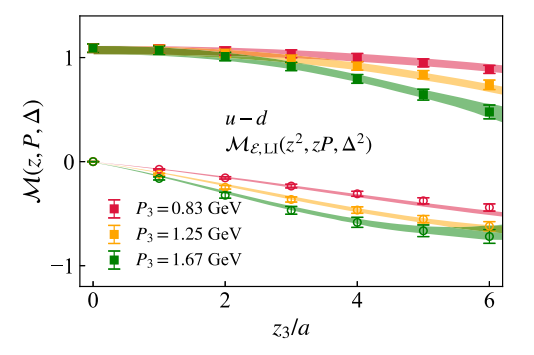


FIG. 8. The combined fit results from $z_3 \in [2a, 6a]$ for $\mathcal{M}_{\mathcal{H}, \mathrm{LI}}$ (left panel) and $\mathcal{M}_{\mathcal{E}, \mathrm{LI}}$ (right panel) at the momentum transfer $-t = 0.69 \; \mathrm{GeV^2}$, as a function of z_3 and using NNLO matching. We have three different momentum $P_3 = 0.83$, 1.25 and 1.67 GeV for this -t. The filled squared symbols are for the real part, while the circled open symbols are for the imaginary part.

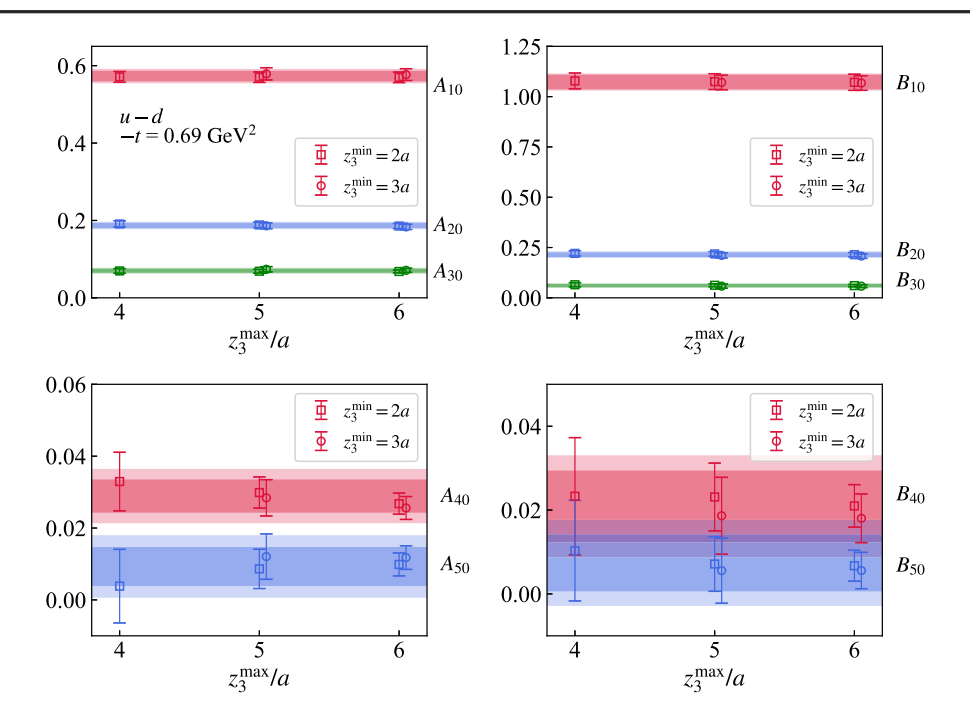


FIG. 9. The first three moments of $A_{n+1,0}$ (left panels) and $B_{n+1,0}$ (right panels) extracted from $z_3^{\min} = 2a$, 3a of $\mathcal{M}_{\mathcal{H},\mathrm{LI}}$ and $\mathcal{M}_{\mathcal{E},\mathrm{LI}}$ using NNLO matching, as a function of z_3^{\max} . We vary $z_3^{\min} = 2a$, 3a and $z_3^{\max} = 4a$, 5a, 6a to estimate the statistical errors as the darker bands and the systematic errors as the lighter bands. The momentum transfer is -t = 0.69 GeV².

the higher moments, one need to increase the hadron momentum to achieve larger zP.

V. -t DEPENDENCE OF THE MELLIN MOMENTS

The Mellin moments of GPDs encapsulate a wealth of physics pertaining to the structure of the nucleon. The first moments A_{10} and B_{10} are Dirac and Pauli form factors. At zero momentum transfer, -t=0, the $A_{10}(0)$ is the total charge carried by the quarks. In addition, one can alternatively define the so-called Sachs electric and magnetic form factors $G_E(-t)=A_{10}(-t)+B_{10}(-t)$ and $G_M(-t)=A_{10}(-t)+-t/(2m_N)^2B_{10}(-t)$, then infer the electric and magnetic radius of the nucleon. It is the second moments A_{20} and B_{20} that have attracted a lot of interest in recent years due to their connection to the gravitational form factors (GFFs), which are the matrix elements of QCD energy-momentum tensor,

$$\langle p_{f} | \hat{T}_{\text{QCD}}^{\mu\nu} | p_{i} \rangle = \bar{u}(p_{f}) \left[A_{20}(t) \gamma^{(\mu} \bar{P}^{\nu)} + B_{20}(t) \frac{\bar{P}^{(\mu} i \sigma^{\nu)\alpha} \Delta_{\alpha}}{2M} + C_{20}(t) \frac{\Delta^{\mu} \Delta^{\nu} - g^{\mu\nu} \Delta^{2}}{4M} \right] u(p_{i}), \tag{26}$$

where C_{20} term can also be extracted from nonzero skewness GPDs. At zero momentum transfer, -t = 0, A_{20} provides information on the momentum fraction carried by the quarks inside the nucleon. Moreover, combining A_{20}

and B_{20} , one can infer the total angular momentum carried by quarks via the Ji sum rule [2],

$$J = \frac{1}{2}(A_{20}(0) + B_{20}(0)). \tag{27}$$

To obtain these quantities, we need to extrapolate the moments to $-t \to 0$, particularly for $B_{n+1,0}$ using a parametrization of choice. It is known that at low momentum transfer -t, the nucleon electromagnetic form factors can be well described by the dipole form,

$$\langle x^n \rangle (-t) = \frac{\langle x^n \rangle (0)}{\left(1 + \frac{-t}{M^2}\right)^2}.$$
 (28)

However, at large -t, there is no strong theoretical support for this simple form. A more flexible parametrization could be the z-expansion [144],

$$\langle x^n \rangle (-t) = \sum_{k=0}^{k_{\text{max}}} a_k z(t)^k, \tag{29}$$

with

$$z(t) = \frac{\sqrt{t_{\text{cut}} - t} - \sqrt{t_{\text{cut}} - t_0}}{\sqrt{t_{\text{cut}} - t} + \sqrt{t_{\text{cut}} - t_0}},$$
(30)

where the parameter $t_{\rm cut}$ is the timelike kinematic threshold for particle production: $t_{\rm cut} = 9m_\pi^2$ for isoscalar form

factors and $t_{\rm cut}=4m_\pi^2$ for isovector form factors. The t_0 is usually chosen to ensure $0 < -t < -t_{\text{max}}$ corresponding to the smallest range of z(-t), which is $t_0^{\text{opt}}(t_{\text{cut}}, -t_{\text{max}}) =$ $t_{\rm cut}(1-\sqrt{1-t_{\rm max}/t_{\rm cut}})$. The $k_{\rm max}$ needs to be truncated at a finite value according to the range of -t. We truncated $k_{\rm max}$ up to 2 in this work with reasonable $\chi^2/{\rm dof}$. To stabilize the fit, we imposed a Gaussian prior to the $|a_k/a_0|$ with central value of 0 and width $|a_k/a_0|_{\text{max}} = 5$. In our analysis, as discussed later, we found both dipole and z-expansion can reasonably describe all of our data with $\chi^2/\text{dof ranging from 0.4 to 1.9. However, we note that}$ these two functional forms are designed for the first moments, so they may not be optimal for the higher moments. Therefore, we vary the fit range of -t as well as the model to estimate the systematic errors using the method described in Sec. IV C. In addition, we stick to the quasi-GPDs in the Lorentz-invariant definition in this section.

A. The model fit and $-t \rightarrow 0$ extrapolation

In Fig. 10, we show the first moments A_{10} and B_{10} extracted from Lorentz-invariant quasi-GPDs, for the isovector (upper panels) as well as the isoscalar (lower panels) cases. The errors included are both statistical and systematic. We also show the results from a direct calculation [145] by ETMC of matrix elements of the local current $\bar{q}(0)\gamma^{\mu}q(0)$, which have been obtained in the rest frame with similar lattice setup. We observe good agreement between the results. We fit the -t dependence using the dipole form as well as the z-expansion form (zExp) shown

as the bands. Two ranges of -t are used with $-t_{\text{max}} = 1.0$ and 1.5 GeV², as our data are sparse in large -t region, and we are more interested in the small -t behavior. We will treat the difference from various $-t_{\text{max}}$ as a source of systematic errors. As can be seen, all the bands can describe well the data included in the fit and overlap with each other in the region of small -t. However, the dipole form, being a simpler expression, tends to yield smaller errors. It is interesting to note that the dipole form is also able to extrapolate to larger values of -t effectively and remains consistent with data points beyond 2 GeV². On the other hand, the z-expansion, which takes the form of polynomial functions of z(-t), tends to become unstable rapidly during the extrapolation. This causes the z-expansion fit to show larger errors and potentially deviate from data points that require long-distance extrapolation. In Table II, we summarize the $-t \rightarrow 0$ extrapolation results, where we take the same strategy as described in Sec. IV C to estimate the statistical and systematic uncertainties from the variation of $-t_{\text{max}}$ and two different models. As one can see, the $A_{10}^{u-d}(0)$, which measures the isovector charge of the nucleon, is close to the expected value of 1. However, our estimation of the isoscalar charge A_{10}^{u+d} using the large momentum matrix element has a $2-\sigma$ deviation with a value of 3, whereas the result from the rest frame matrix elements as discussed in Appendix B is very close to the expectation. This discrepancy could be due to the discretization effect that occurs for highly boosted hadron states [89]. In addition, one can observe good agreement between our $B_{10}^{u-d}(0)$ with the ETMC'11 results, while the $B_{10}^{u+d}(0)$ are

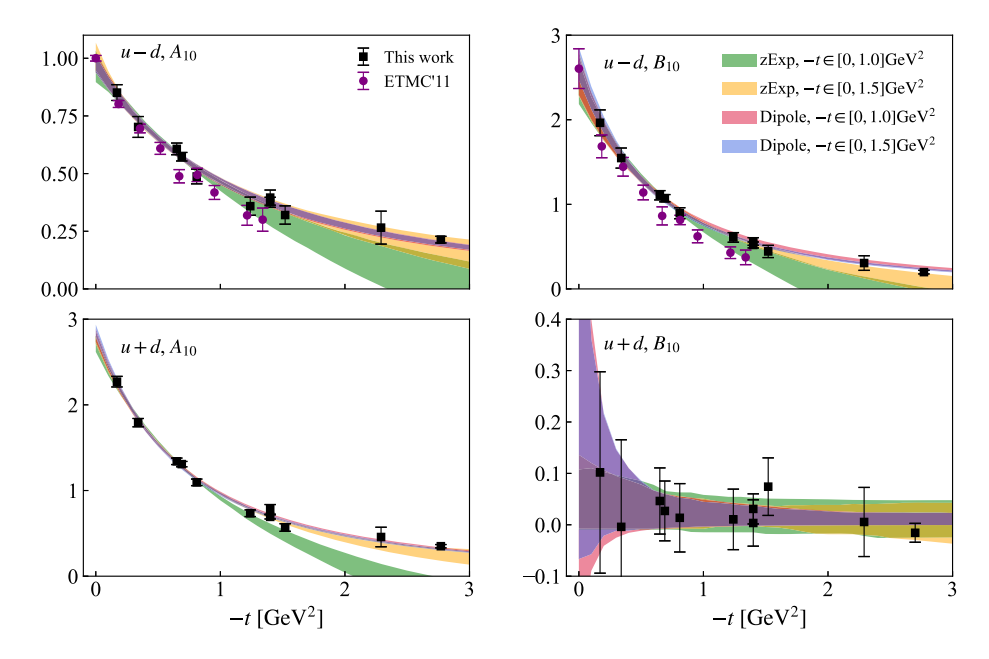


FIG. 10. The first moments A_{10} and B_{10} for isovector (upper panels) and isoscalar (lower panels) as a function of -t. The error bars include both statistical errors and systematic errors. The bands come from two different parametrizations using two ranges of -t. For comparison, we also show the ETMC determination of isovector moments with a similar lattice setup [145].

$-t \to 0$	This work	ETMC'11 [145]	$-t \rightarrow 0$	This work	ETMC'11 [35]
A_{10}^{u-d}	0.982(47)(28)	1	A_{20}^{u-d}	0.267(13)(10)	0.264(13)
A_{10}^{u+d}	2.786(78)(64)		A_{20}^{u+d}	0.544(15)(06)	0.613(14)
B_{10}^{u-d}	2.540(221)(108)	2.61(23)	B_{20}^{u-d}	0.295(38)(23)	0.301(47)
B_{10}^{u+d}	0.170(299)(290)		B_{20}^{u+d}	0.047(33)(65)	-0.046(43)

TABLE II. The first two moments extrapolated to $-t \to 0$ are shown. For comparison, we also show the first and second moments from the ETMC determination with similar lattice setup [35,145].

consistent with zero within the errors, as has been observed at the level of bare matrix elements in Fig. 2.

In Fig. 11, we show the gravitational form factors A_{20} and B_{20} as a function of -t for the isovector (upper panels) as well as the isoscalar (lower panels) cases. Good agreement can be found by comparing our results to those obtained from traditional calculations of local operators with one covariant derivative and a similar lattice setup (ETMC'11) [35]. Building upon our findings in Sec. IV B, this further strengthens our confidence for the quasi-GPDs, particularly for \mathcal{E} quasi-GPDs, under our Lorentz-invariant definition [118], having smaller power corrections and good perturbative convergence to the light-cone GPDs. Moreover, the bands resulting from different fits can capture well all the data points within the fit, where the dipole form typically exhibits more stability and smaller errors with fewer parameters. The $-t \rightarrow 0$ extrapolation results are summarized in Table II, in which the $A_{20}(0)$ can be interpreted as the hadron momentum fraction carried by the isovector and isoscalar quarks. Our results for isovector cases agree well with the determination from ETMC'11 [35], while a mild deviation is again observed for the A_{20}^{u+d} , possibly due to the discretization effect [89], and the mixing with gluons that is not accounted for in the SDF [142]. We also note that this work used less than half the amount of configurations compared to Ref. [35] and the time separation $t_s = 10a$ is also smaller ($t_s = 12a$ in Ref. [35]). Using the gravitational form factors extrapolated at -t = 0, we evaluate the spin contribution of the nucleon from the isovector and isoscalar quarks as indicated by Eq. (27), which are,

$$J^{u-d} = 0.281(21)(11),$$

 $J^{u+d} = 0.296(22)(33),$ (31)

The errors in the first and second parenthesis are the usual statistical errors and systematic errors described above. We note that the NNLO and NLO matching kernels are used for isovector and isoscalar cases, respectively. Our determination is consistent with the existing results of ETMC [35]; however, we note that the quark masses of this exploratory

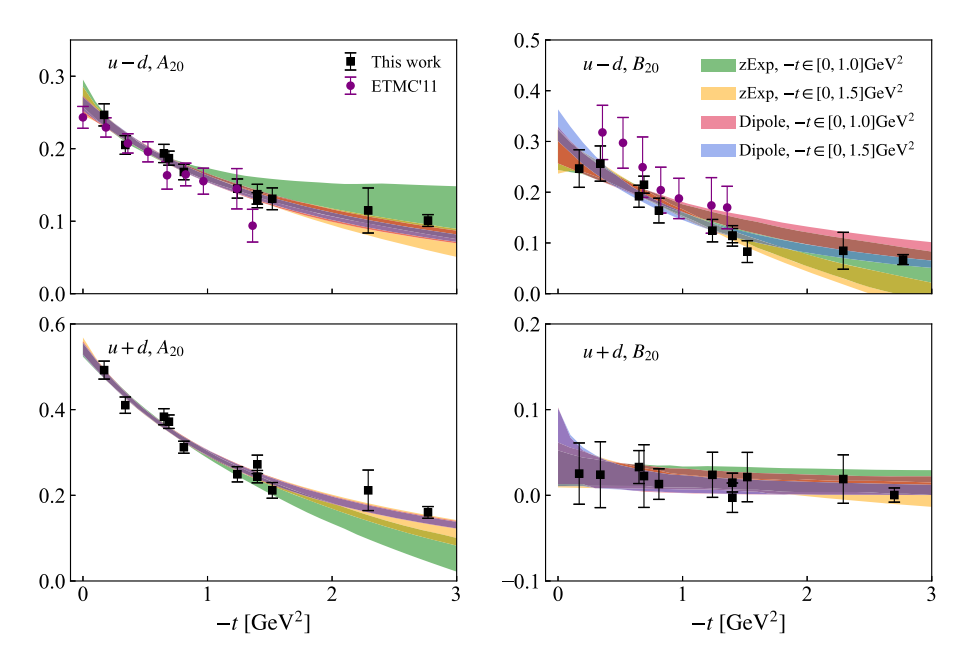


FIG. 11. The second moments A_{20} and B_{20} for isovector (upper panels) and isoscalar (lower panels) as a function of -t. The error bars include both statistical errors and systematic errors. The bands come from two different parametrizations using two ranges of -t. For comparison, we also show the ETMC determination of isovector moments with a similar lattice setup [35].

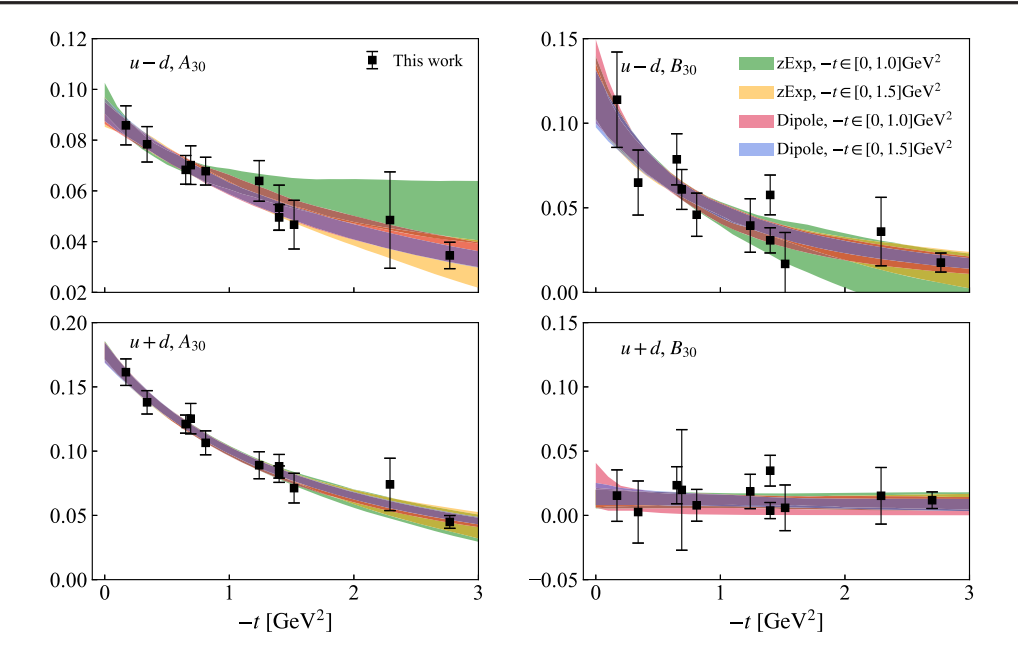


FIG. 12. The third moments A_{30} and B_{30} for isovector (upper panels) and isoscalar (lower panels) as a function of -t. The error bars include both statistical errors and systematic errors. The bands come from two different parametrizations using two ranges of -t.

calculation are not at the physical point, and we also need more studies to address the lattice discretization errors and the excited state contamination in the future.

We show the third, fourth, and fifth moments, for the first time, as a function of -t in Figs. 12–14. Reasonable signal and smooth -t dependence can be observed for the $A_{n+1,0}$ moments, while the isovector B_{50} and all the isoscalar $B_{n+1,0}$ moments are mostly consistent with zero. All the

results are also summarized in Appendix A. There are no existing results for comparison, which, however, is essentially the advantage of the method used in this work, namely the short distance factorization of quasi-GPD matrix element, that one can systematically get access to the higher moments with larger hadron momentum. On the contrary, the traditional moments calculations are limited to the lowest few moments, as discussed previously.

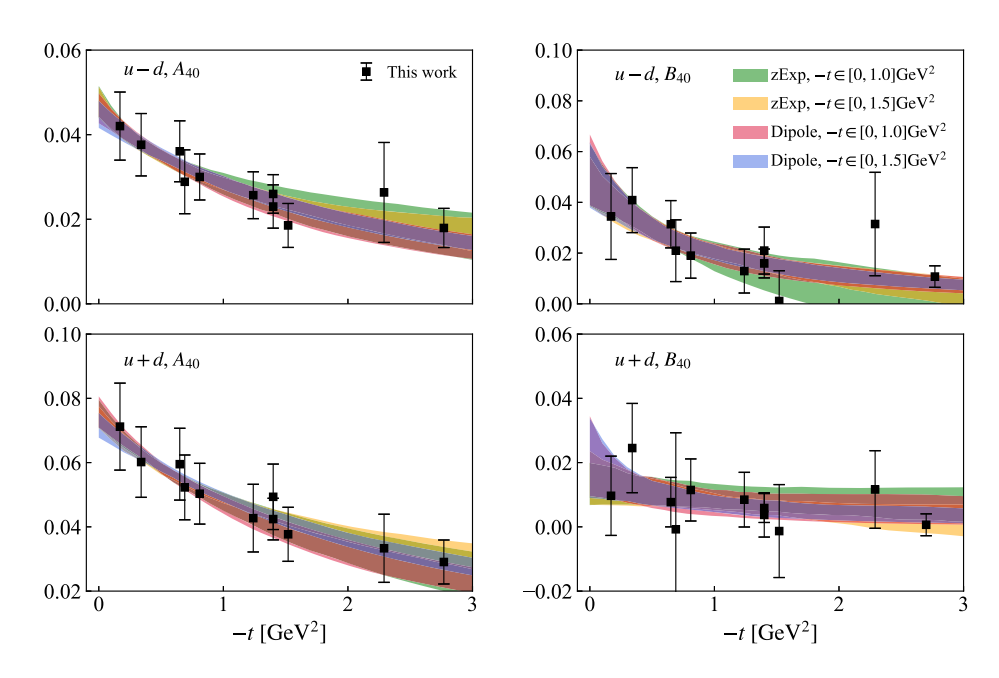


FIG. 13. The fourth moments A_{40} and B_{40} for isovector (upper panels) and isoscalar (lower panels) as a function of -t. The error bars include both statistical errors and systematic errors. The bands come from two different parametrizations using two ranges of -t.

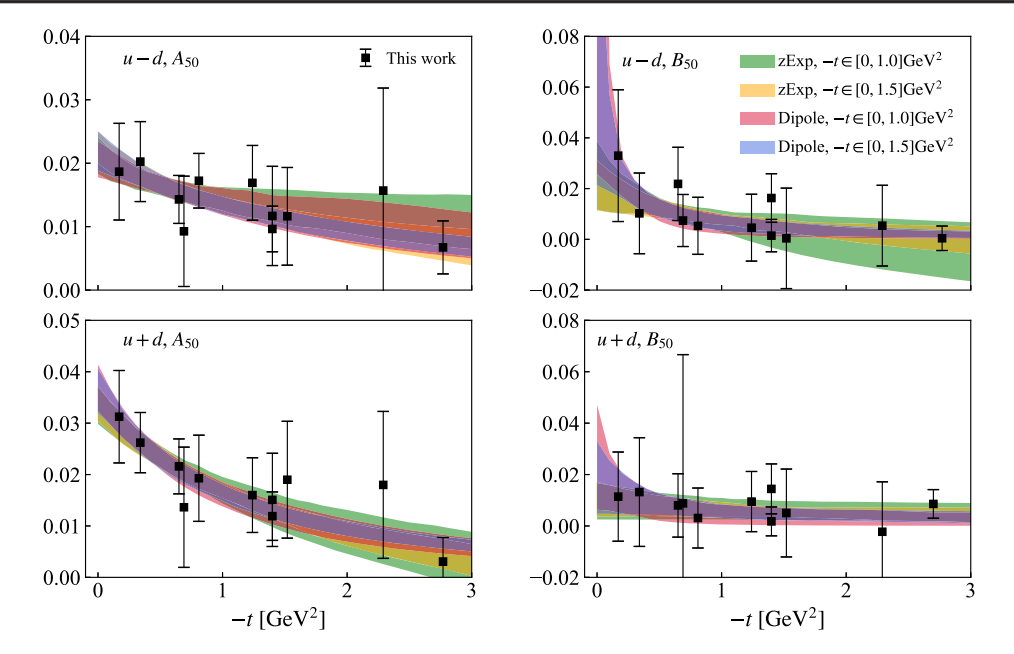


FIG. 14. The fifth moments A_{50} and B_{50} for isovector (upper panels) and isoscalar (lower panels) as a function of -t. The error bars include both statistical errors and systematic errors. The bands come from two different parametrizations using two ranges of -t.

Moreover, it is notable that the moments of each type of $A_{n+1,0}$ and $B_{n+1,0}$ show a qualitative hierarchy that is consistent with the large N_c counting rules [146],

$$\begin{split} |A_{n+1,0}^{u+d}| \sim N_c^2 \gg |A_{n+1,0}^{u-d}| \sim N_c, \\ |B_{n+1,0}^{u-d}| \sim N_c^3 \gg |B_{n+1,0}^{u+d}| \sim N_c^2. \end{split} \tag{32}$$

However, we also note a breaking of the prediction between different types, consistent with previous findings [52],

$$|B_{n+1,0}^{u-d}| \sim N_c^3 \gg |A_{n+1,0}^{u+d}| \sim N_c^2.$$
 (33)

Specifically, our results show that $A_{n+1,0}^{u-d} \gtrsim B_{n+1,0}^{u-d}$.

B. Impact parameter space interpretation

The GPDs can be interpreted in the impact parameter space, with the zero-skewness GPDs being particularly relevant. Specifically, when considering unpolarized quarks inside an unpolarized proton, the Fourier transform of the H GPDs provides information on how partons carrying a momentum fraction x are distributed in the transverse plane,

$$q(x, \vec{b}_{\perp}) = \int \frac{d^2 \vec{\Delta}_{\perp}}{(2\pi)^2} H(x, -\vec{\Delta}_{\perp}^2) e^{-i\vec{b}_{\perp} \cdot \vec{\Delta}_{\perp}}.$$
 (34)

Taking into account the E GPDs, one can explore the unpolarized quarks distribution inside a transversely polarized proton [7], defined as,

$$q^{T}(x, \vec{b}_{\perp})$$

$$= \int \frac{d^{2}\vec{\Delta}_{\perp}}{(2\pi)^{2}} \left[H(x, -\vec{\Delta}_{\perp}^{2}) + i \frac{\Delta_{y}}{2M} E(x, -\vec{\Delta}_{\perp}^{2}) \right] e^{-i\vec{b}_{\perp} \cdot \vec{\Delta}_{\perp}}$$

$$= q(x, \vec{b}_{\perp}) - \frac{1}{2M} \frac{\partial}{\partial b_{y}} q_{E}(x, \vec{b}_{\perp}), \tag{35}$$

where we denoted the Fourier transform of $E(x, -\vec{\Delta}^2)$ by $q_E(x, \vec{b}_\perp)$, and the proton is transversely polarized in the x direction. These impact parameter-dependent parton distributions (IPDs) allow us to visualize the three-dimensional structure of the parton distribution inside the proton, taking into account both longitudinal momentum and transverse position. The $q^T(x, \vec{b}_\perp)$ also have a relation to the Sivers distributions [147–149]. In this work, we derived the moments of the H and E GPDs, which enabled us to infer the moments of $q(x, \vec{b}_\perp)$ and $q^T(x, \vec{b}_\perp)$,

$$\rho_{n+1}(\vec{b}_{\perp}) = \int \frac{d^{2}\vec{\Delta}_{\perp}}{(2\pi)^{2}} A_{n+1,0}(-\vec{\Delta}_{\perp}^{2}) e^{-i\vec{b}_{\perp}\cdot\vec{\Delta}_{\perp}},$$

$$\rho_{n+1}^{T}(\vec{b}_{\perp}) = \int \frac{d^{2}\vec{\Delta}_{\perp}}{(2\pi)^{2}} \left[A_{n+1,0}(-\vec{\Delta}_{\perp}^{2}) + i \frac{\Delta_{y}}{2M} B_{n+1,0}(-\vec{\Delta}_{\perp}^{2}) \right] e^{-i\vec{b}_{\perp}\cdot\vec{\Delta}_{\perp}}.$$
(36)

Since Fourier transforms require full information of $-t \in [0, \infty]$, we utilized our dipole fit result from $-t \in [0, 1.5]$ GeV², which was found to describe the data up to 2.77 GeV² and will model the $-t \to \infty$ behavior.

We excluded the contribution from $B_{n+1,0}^{u+d}$, as these data were mostly consistent with zero in our calculations. We then will compute the impact space distribution for up and down quarks as a function of \vec{b}_{\perp} for both $\rho_{n+1}(\vec{b}_{\perp})$ and $\rho_{n+1}^T(\vec{b}_\perp)$, with n ranging from 0 to 3. We excluded the n=4 case since B_{50}^{u+d} and B_{50}^{u-d} are both noisy and consistent with 0, although a reasonable signal was observed for A_{50}^{u+d} and A_{50}^{u-d} . The flavor separation is derived by a linear combination of our isovector and isoscalar results. We note again that our analysis did not account for the disconnected diagram contributions or mixing with gluons in the isoscalar case, which are expected to be small and not significantly impact our qualitative findings [92]. Additionally, it is worth noting that the moments of the IPDs receive contributions from both quarks and antiquarks, with an integral taken from x = -1 to 1. The difference or sum of the quark and antiquark density distributions can be denoted as ρ_{n+1} = $\rho_{n+1}^q + (-1)^{n+1} \rho_{n+1}^{\bar{q}}$ for even or odd n, respectively [150].

In the upper left panel of Fig. 15, we present the first moments ρ_1 (left) and ρ_1^T (right), which describe the density distribution of up and down quarks in the transverse plane. As one can see, the down quark exhibits a broader distribution and smaller amplitudes compared to the up quark in the unpolarized proton. When the proton is transversely polarized, the up and down quarks shift in different directions, with the down quarks showing larger distortion. This observation holds true for cases when n > 0, where the density distribution is weighted by x^n . The second moment, in particular, is of interest as it describes how momentum is distributed in the transverse plane. The larger distortion of down quarks can be attributed to the fact that they constitute a smaller fraction of the proton, as indicated by the $|A_{n+1,0}^u| > |A_{n+1,0}^d|$, but are subject to similar distortion forces, as evidenced by $B_{n+1,0}^u \approx -B_{n+1,0}^d$. This also ensures that the total contribution of u and d quarks to the transverse center of momentum, $\sum_{u,d} \int d^2 \vec{b}_{\perp} b_y \rho_2(\vec{b}_{\perp}) = 1/(2M) B_{20}^{u+d}(-t=0)$, is approximately 0. Therefore, it is reasonable to expect that

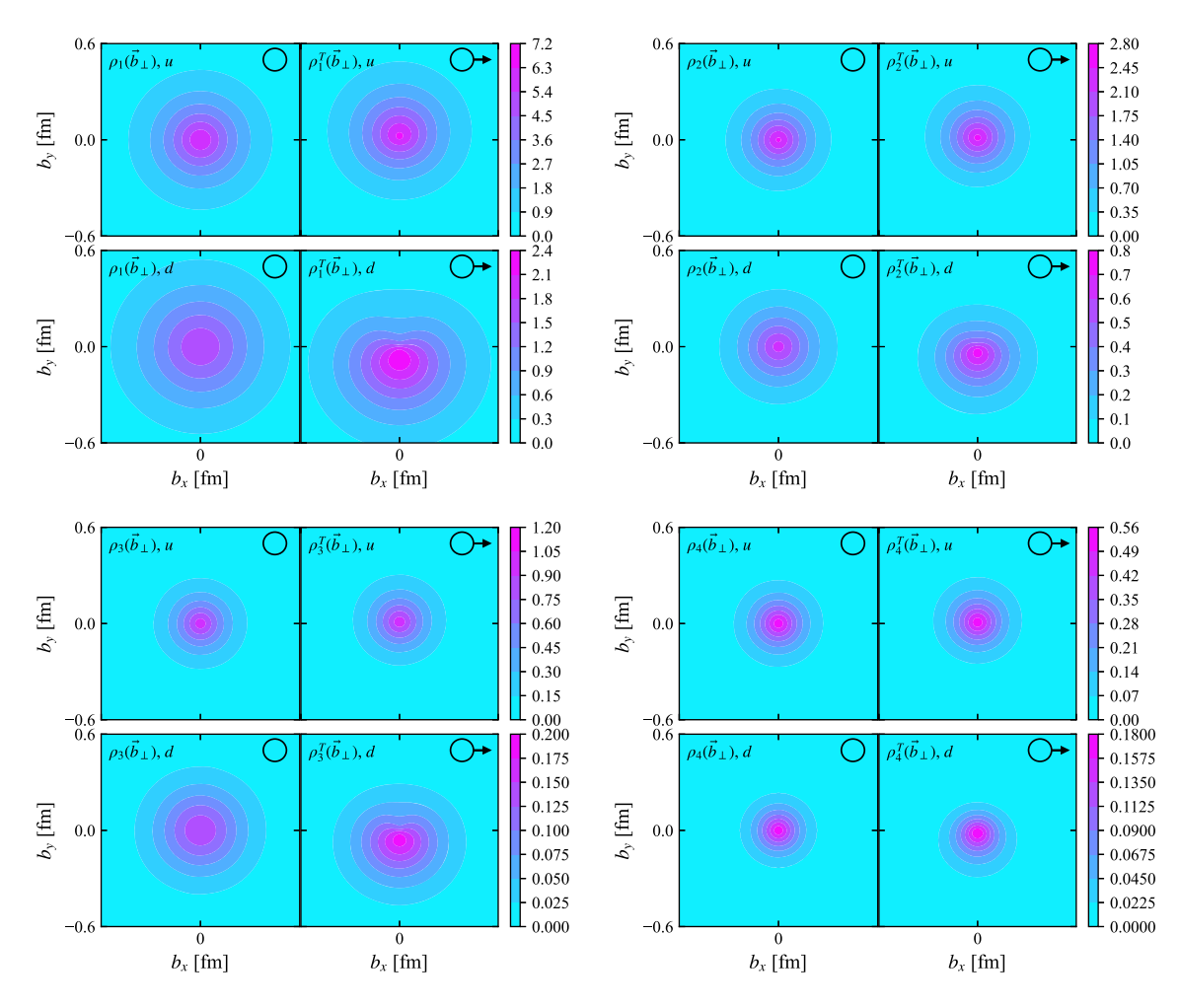


FIG. 15. The first four moments of impact parameter parton distributions in the transverse plane. The unpolarized and transversely polarized (in x direction) proton are both shown in the left and right parts of each panels, denoted by $\rho_{n+1}[\text{fm}^{-2}]$ and $\rho_{n+1}^{T}[\text{fm}^{-2}]$ for both up (u) and down (d) quarks.

the shift of gluon distribution in a transversely polarized proton would be either close 0 or counterbalanced by heavier sea quarks and the contributions from the disconnected diagrams of light quarks. What is more, one can find that ρ_{n+1} (and ρ_{n+1}^T) with higher n exhibit a sharper drop in the transverse distance for even and odd moments, indicating that active quarks with larger x may be more concentrated around the center than small-x quarks inside the proton.

VI. CONCLUSION

In this work, we present the first lattice calculation of the Mellin moments of nucleon unpolarized quark generalized parton distributions (GPDs) up to the fifth order. We utilize the short distance factorization of quasi-GPD matrix elements, calculating both isovector and isoscalar combinations, while ignoring the contribution of disconnected diagrams and quark-gluon mixing to the isoscalar case. Our calculation was carried out using one ensemble of $N_f = 2 + 1 + 1$ twisted mass fermions with clover improvement, where the pion mass was set to 260 MeV and the lattice spacing was a = 0.093 fm. We calculate the bare quasi-GPDs in both asymmetric and symmetric frames using the γ_0 definition and construct the ones of a recently proposed Lorentz-invariant definition [118]. We renormalize the bare matrix elements using the zero-momentum quasi-PDF matrix elements through the ratio scheme. By inserting the SDF formula into the RG-invariant ratio-scheme matrix elements, we can extract the Mellin moments with perturbatively calculated Wilson coefficients up to NNLO for the isovector case and up to NLO for the isoscalar case. To test the validity of the approach we first performed analysis at fixed z_3 varying only P_3 , and studied how the results change when we choose different values of z_3 . In the case of the Lorentz-invariant definition, within the statistical error our results on the moments show no z₃-dependence with NLO/NNLO Wilson coefficients as compared to the slight z_3 -dependence at LO, implying that matching can account for the small-z₃ evolution effects and that the higher-twist contributions are negligible. In the isovector case there is no apparent difference between NLO and NNLO during the numerical implementation, given the current statistics, implying that the higher order corrections are small compared to the statistical errors. However, we find that for the quasi GPDs \mathcal{E} with the γ_0 definition the short distance factorization does not seem to work even if NNLO matching coefficients are used. We then conducted a combined analysis by fitting a range of z values and incorporating the evolution kernels, which enabled us to obtain reliable results for the moments up to the fifth order using the Lorentz-invariant quasi-GPDs, as detailed in Sec. IV C. Notably, the first two moments under the Lorentz-invariant definition consistently agree with traditional moment calculations. This may be an indication that the quasi-GPDs, at least for \mathcal{E} , from Lorentz-invariant definition have potentially smaller power corrections and converge to the light-cone GPDs faster. In Sec. V, we presented, for the first time up to fifth order, moments from both the isovector and isoscalar quasi-GPDs, with various values of momentum transfer -t. We benefited greatly from the short-distance factorization of the quasi-GPD matrix elements, which allowed us to systematically access higher moments by increasing the hadron momentum. Then we applied two methods of fit using the dipole model and z-expansion formula and found them both describe well the -t dependence of the moments we got. From the fit results, we were able to infer the moments for $-t \rightarrow 0$, as well as the quark charges, momentum fraction, and total angular momentum contributions to the proton spin. These are all crucial quantities for understanding the structure of the nucleon. Finally, we discuss the impact parameter space interpretation of the GPDs and their moments by Fourier transform the dipole fit results, which provides insights into the spatial distribution of quarks and their correlations in the transverse plane of an unpolarized or transversely polarized proton. In future work, we will refine calculations at the physical point and investigate systematic uncertainties such as discretization effects and excited state contamination, and possibly further constrain the higher moments with better data quality.

ACKNOWLEDGMENTS

This material is based upon work supported by the U.S. Department of Energy, Office of Science, Office of Nuclear Physics through Contract No. DE-SC0012704, No. DE-AC02-06CH11357 and within the framework of Scientific Discovery through Advance Computing (SciDAC) award Fundamental Nuclear Physics at the Exascale and Beyond. S. B. is supported by Laboratory Directed Research and Development (LDRD) funds from Brookhaven Science Associates. K.C. is supported by the National Science Centre (Poland) grants SONATA BIS No. 2016/22/E/ST2/ 00013 and OPUS No. 2021/43/B/ST2/00497. M.C., J.D., and A. S. acknowledge financial support by the U.S. Department of Energy, Office of Nuclear Physics, Early Career Award under Grant No. DE-SC0020405. The work of A. M. is supported by the National Science Foundation under Grant No. PHY-2110472, and also by the U.S. Department of Energy, Office of Science, Office of Nuclear Physics, within the framework of the TMD Topical Collaboration. F. S. was funded by the NSFC and the Deutsche Forschungsgemeinschaft (DFG, German Research Foundation) through the funds provided to the Sino-German Collaborative Research Center TRR110 "Symmetries and the Emergence of Structure in QCD" (NSFC Grant No. 12070131001, DFG Project-ID 196253076—TRR 110). The authors also acknowledge partial support by the U.S. Department of Energy, Office of Science, Office of Nuclear Physics under the umbrella of the Quark-Gluon Tomography (QGT) Topical Collaboration with Award DE-SC0023646. This publication is partially funded by the Gordon and Betty Moore Foundation through the Grant GBMF6210 to APS to support the participation and presentation of X. G. at the 10th APS GHP meeting (April 12-14, 2023). Computations for this work were carried out in part on facilities of the USQCD Collaboration, which are funded by the Office of Science of the U.S. Department of Energy. This research used resources of the Oak Ridge Leadership Computing Facility, which is a DOE Office of Science User Facility supported under Contract No. DE-AC05-00OR22725. This research was supported in part by PLGrid Infrastructure (Prometheus supercomputer at AGH Cyfronet in Cracow). Computations were also partially performed at the Poznan Supercomputing and Networking

Center (Eagle supercomputer), the Interdisciplinary Centre for Mathematical and Computational Modelling of the Warsaw University (Okeanos supercomputer), and at the Academic Computer Centre in Gdańsk (Tryton supercomputer). The gauge configurations have been generated by the Extended Twisted Mass Collaboration on the KNL (A2) Partition of Marconi at CINECA, through the Prace project Pra13_3304 "SIMPHYS". Inversions were performed using the DD-αAMG solver [151] with twisted mass support [152].

APPENDIX A: TABLES OF THE MOMENTS

We list all our determination of GPD moments in Tables III–VI. The factorization scale is set to be $\mu=2$ GeV.

TABLE III. The table of isovector GPD moments $A_{n+1,0}^{u-d}$.

−t GeV ²	A_{10}^{u-d}	A_{20}^{u-d}	A_{30}^{u-d}	A_{40}^{u-d}	A_{50}^{u-d}
0.17	0.851(31)(03)	0.247(11)(04)	0.086(04)(03)	0.042(03)(05)	0.019(03)(05)
0.34	0.702(43)(02)	0.205(01)(03)	0.078(05)(02)	0.038(03)(04)	0.020(03)(03)
0.65	0.607(24)(01)	0.193(09)(04)	0.068(05)(01)	0.036(02)(05)	0.014(02)(02)
0.69	0.573(14)(04)	0.187(07)(03)	0.070(05)(02)	0.029(05)(03)	0.009(05)(03)
0.81	0.487(31)(01)	0.168(09)(02)	0.068(04)(01)	0.030(03)(03)	0.017(03)(02)
1.24	0.359(37)(02)	0.145(12)(01)	0.064(06)(02)	0.026(04)(02)	0.017(03)(03)
1.38	0.396(03)(03)	0.137(12)(02)	0.053(06)(03)	0.023(03)(02)	0.012(04)(04)
1.38	0.376(21)(01)	0.129(09)(02)	0.050(04)(01)	0.026(02)(02)	0.010(02)(01)
1.52	0.320(37)(03)	0.131(14)(01)	0.047(07)(03)	0.019(04)(01)	0.012(04)(04)
2.29	0.266(66)(05)	0.115(28)(03)	0.048(14)(05)	0.026(08)(04)	0.016(08)(08)
2.77	0.214(13)(01)	0.101(07)(01)	0.035(04)(01)	0.018(03)(02)	0.007(03)(02)

TABLE IV. The table of isovector GPD moments $B_{n+1,0}^{u-d}$.

$-t \text{ GeV}^2$	B_{10}^{u-d}	B_{20}^{u-d}	B_{30}^{u-d}	B_{40}^{u-d}	B_{50}^{u-d}
0.17	1.964(142)(011)	0.247(33)(04)	0.114(17)(11)	0.034(11)(05)	0.033(09)(17)
0.34	1.547(113)(006)	0.256(32)(03)	0.065(13)(06)	0.041(08)(04)	0.010(08)(08)
0.65	1.107(49)(06)	0.192(18)(03)	0.079(09)(06)	0.031(05)(04)	0.022(06)(09)
0.69	1.073(37)(06)	0.215(12)(05)	0.061(08)(03)	0.021(09)(04)	0.007(07)(03)
0.81	0.895(61)(03)	0.164(23)(02)	0.046(09)(04)	0.019(07)(02)	0.005(06)(05)
1.24	0.609(52)(04)	0.124(20)(02)	0.040(11)(05)	0.013(06)(03)	0.005(06)(07)
1.38	0.561(42)(03)	0.114(18)(02)	0.058(09)(03)	0.021(06)(03)	0.016(05)(04)
1.38	0.520(33)(02)	0.114(13)(01)	0.031(05)(02)	0.016(04)(02)	0.001(03)(03)
1.52	0.443(65)(07)	0.083(19)(02)	0.017(11)(07)	0.001(09)(03)	0.000(09)(11)
2.29	0.306(81)(05)	0.085(32)(04)	0.036(15)(05)	0.031(15)(05)	0.005(09)(07)
2.77	0.199(19)(02)	0.067(09)(01)	0.018(04)(02)	0.011(03)(01)	0.000(03)(02)

TABLE V. The table of isoscalar GPD moments $A_{n+1,0}^{u+d}$.

−t GeV ²	A_{10}^{u+d}	A_{20}^{u+d}	A_{30}^{u+d}	A_{40}^{u+d}	A_{50}^{u+d}
0.17	2.271(58)(04)	0.492(14)(07)	0.161(06)(04)	0.071(03)(01)	0.031(04)(05)
0.34	1.792(47)(01)	0.410(13)(06)	0.138(08)(01)	0.060(03)(08)	0.026(04)(02)
0.65	1.341(36)(02)	0.383(12)(06)	0.121(06)(02)	0.060(03)(09)	0.022(03)(02)
0.69	1.308(20)(12)	0.372(11)(05)	0.125(06)(05)	0.052(06)(05)	0.014(06)(05)

(Table continued)

TABLE V. (Continued)

−t GeV ²	A_{10}^{u+d}	A_{20}^{u+d}	A_{30}^{u+d}	A_{40}^{u+d}	A_{50}^{u+d}
0.81	1.095(36)(03)	0.312(01)(04)	0.106(06)(03)	0.050(04)(06)	0.019(04)(05)
1.24	0.735(37)(02)	0.249(13)(04)	0.089(08)(02)	0.043(04)(06)	0.016(04)(03)
1.38	0.780(53)(03)	0.272(17)(04)	0.088(06)(03)	0.049(05)(06)	0.015(04)(05)
1.38	0.692(23)(02)	0.244(12)(03)	0.082(05)(02)	0.042(03)(04)	0.012(02)(02)
1.52	0.568(40)(04)	0.212(16)(02)	0.071(08)(04)	0.038(05)(03)	0.019(05)(06)
2.29	0.457(110)(05)	0.212(46)(02)	0.074(16)(04)	0.033(08)(02)	0.018(08)(06)
2.77	0.350(18)(01)	0.160(11)(03)	0.045(04)(01)	0.029(03)(04)	0.003(03)(02)

TABLE VI. The table of isoscalar GPD moments $B_{n+1,0}^{u+d}$.

−t GeV ²	B_{10}^{u+d}	B_{20}^{u+d}	B_{30}^{u+d}	B_{40}^{u+d}	B_{50}^{u+d}
0.17	0.102(191)(05)	0.025(34)(02)	0.015(15)(05)	0.010(10)(03)	0.011(10)(07)
0.34	-0.004(162)(08)	0.024(35)(04)	0.003(17)(08)	0.025(09)(05)	0.013(10)(11)
0.65	0.046(61)(03)	0.033(18)(02)	0.023(11)(03)	0.008(05)(02)	0.008(07)(05)
0.69	0.027(41)(17)	0.022(30)(07)	0.02(31)(16)	-0.001(19)(11)	0.009(29)(28)
0.81	0.014(63)(04)	0.013(16)(02)	0.008(08)(04)	0.011(07)(02)	0.003(06)(06)
1.24	0.011(56)(03)	0.024(24)(02)	0.019(10)(03)	0.008(06)(03)	0.009(07)(05)
1.38	0.004(42)(03)	-0.003(16)(01)	0.035(09)(03)	0.004(05)(02)	0.014(06)(04)
1.38	0.031(27)(02)	0.015(10)(01)	0.004(04)(02)	0.006(04)(01)	0.002(03)(03)
1.52	0.074(50)(06)	0.021(25)(04)	0.006(12)(06)	-0.001(09)(06)	0.005(08)(09)
2.29	0.005(61)(06)	0.019(26)(03)	0.015(16)(06)	0.012(09)(03)	-0.002(10)(10)
2.77	-0.016(16)(02)	0.000(08)(01)	0.012(04)(02)	0.001(02)(01)	0.009(02)(03)

APPENDIX B: QUASI-PDF MATRIX ELEMENTS AT P=0

In Sec. III B, we take the isovector quasi-PDF matrix elements $\mathcal{F}(\vec{z}, \vec{P}=0, \vec{\Delta})$ for the ratio scheme renormalization. For comparison, we show the isoscalar bare quasi-PDF matrix elements in Fig. 16. It's known that the isovector local matrix element $\mathcal{F}_{u-d}(\vec{z}=0, \vec{P}=0, \vec{\Delta}=0)$ by definition is the vector current renormalization factor,

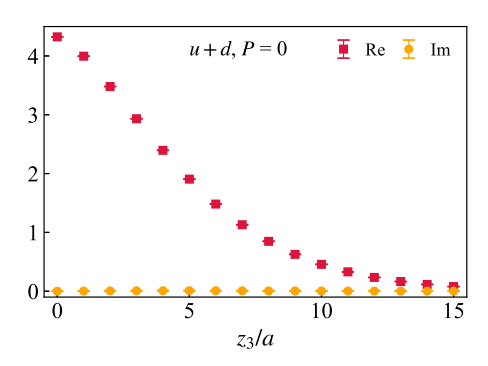


FIG. 16. Bare matrix elements of isoscalar zero-momentum quasi-PDF matrix elements $\mathcal{F}(z, P=0, \Delta=0)$.

which is $Z_V^{-1}=1.440(1)$ as shown in Fig. 3. By utilizing the value $\mathcal{F}_{u+d}(\vec{z}=0,\vec{P}=0,\vec{\Delta}=0)=4.325(1)$, we obtain $Z_V\mathcal{F}_{u+d}(\vec{z}=0,\vec{P}=0,\vec{\Delta}=0)=3.004(2)$, a value which closely approximates the nucleon's isoscalar charge of 3, even though the disconnected diagrams are not accounted for.

Putting aside the difference of over all charges, one can normalize the bare matrix elements for both isovector and isoscalar cases as $\mathcal{F}_{u-d}(\vec{z},\vec{P}=0,\vec{\Delta})/\mathcal{F}_{u-d}(\vec{z}=0,\vec{P}=0,$ $\vec{\Delta} = 0$) and $\mathcal{F}_{u+d}(\vec{z}, \vec{P} = 0, \vec{\Delta}) / \mathcal{F}_{u+d}(z = 0, P = 0, \Delta = 0)$ shown in Fig. 17. As expected, the normalized matrix elements from isovector and isoscalar cases are close to each other. This can be attributed to two reasons: first, the renormalization factor is identical for both cases; and second, after renormalization, the leading order perturbation calculation indicates that they are also approximately the same, disregarding the mixing between isoscalar and gluon matrix elements and considering the Wilson coefficient C_0 at short distances. However, this argument may not hold beyond leading order or when z increases significantly, at which point the isovector and isoscalar cases may begin to diverge.

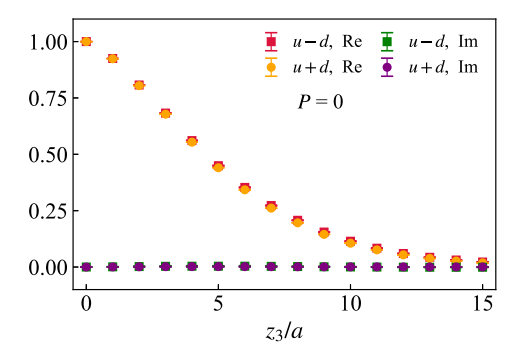


FIG. 17. Normalized bare matrix elements of zero-momentum quasi-PDF matrix elements $\mathcal{F}_{u-d}(\vec{z},\vec{P}=0,\vec{\Delta}=0)/\mathcal{F}_{u-d}(\vec{z}=0,\vec{P}=0,\vec{\Delta}=0)$ and $\mathcal{F}_{u+d}(\vec{z},\vec{P}=0,\vec{\Delta})/\mathcal{F}_{u+d}(\vec{z}=0,\vec{P}=0,\vec{\Delta}=0)$ for both isovector and isoscalar cases.

APPENDIX C: QUASI-GPD MATRIX ELEMENTS IN γ_0 DEFINITION

In Sec. III, we presented the quasi-GPD matrix elements in Lorentz-invariant definition, while here we show all the matrix elements from the γ_0 definition, which have been used in the main text. The bare matrix elements in the asymmetric frame with $\vec{p}_f = \vec{P}^a$ and $\vec{p}_i = \vec{P}^a - \vec{\Delta}^a$ are shown in Fig. 18, and the ones in the symmetric frames with $\vec{p}_f = \vec{P}^s + 1/2\vec{\Delta}^s$ and $\vec{p}_i = \vec{P}^s - 1/2\vec{\Delta}^s$ are shown in Fig. 19. Compared to the Lorentz-invariant definition in Fig. 2, one can find the quasi-GPD matrix elements in γ_0 definitions show some difference, which will result in a deviation of renormalized matrix and subsequently the extracted moments as discussed in the main text.

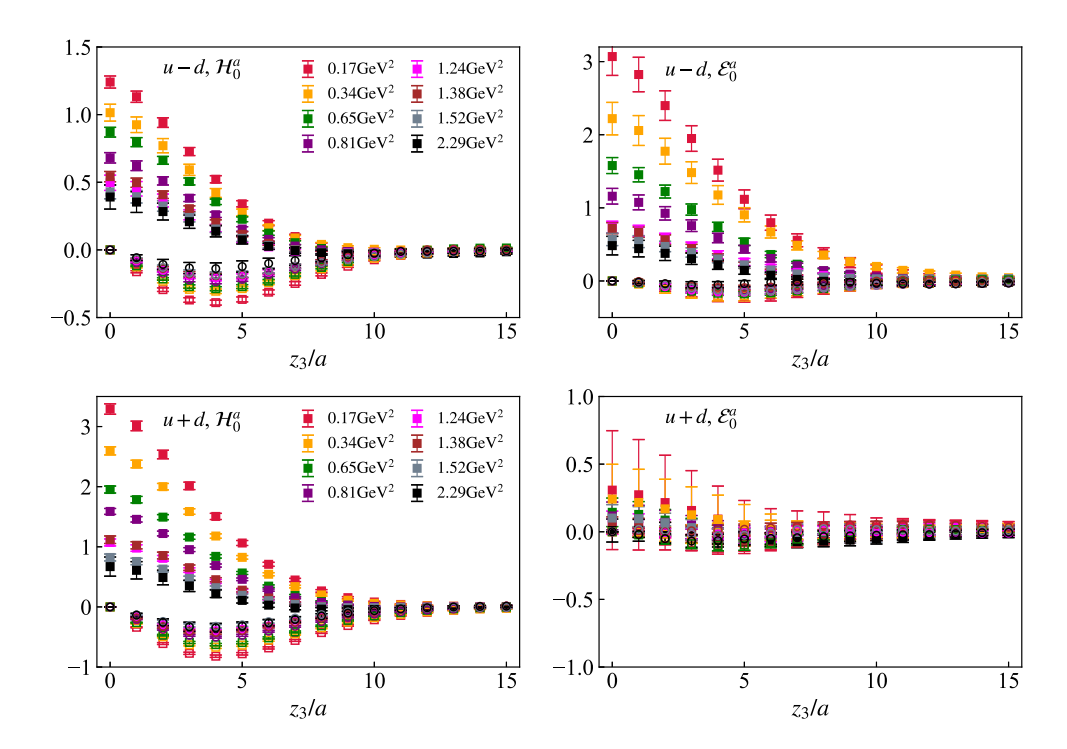


FIG. 18. Bare matrix elements under γ_0 definition from asymmetric frame. The upper and lower panels are for the isovector and isoscalar cases, with squared points for the real part and circled points for the imaginary part. The data shown are from hadron momentum $P_3 = 1.25$ GeV with all the momentum transfer -t we have.

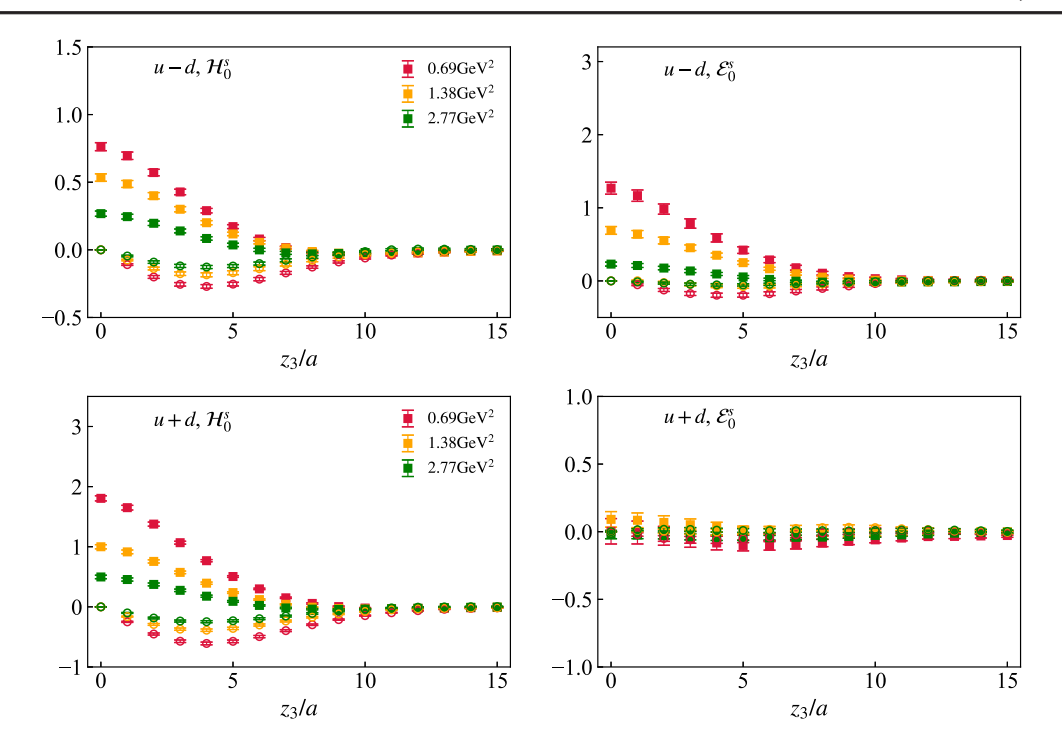


FIG. 19. Bare matrix elements under γ_0 definition from symmetric frame. The upper and lower panels are for the isovector and isoscalar cases, with squared points for real part and circled points for imaginary part. The data shown are from hadron momentum $P_3 = 1.25$ GeV with all the momentum transfer -t we have.

APPENDIX D: MOMENTS EXTRACTION INCLUDING A LEADING-ORDER POWER CORRECTION

As has been mentioned in Sec. IVA, the short distance factorization suffers from power correction $\mathcal{O}(z^2\Lambda_{\rm QCD}^2)$. Thus, one should keep the z^2 at a short distance. The ratioscheme renormalization has the potential to reduce the power correction because of the possible cancellation between the numerator and denominator. In Sec. IV B, we found the leading-twist factorization formula truncated

at $n_{\rm max}=4$ can describe the data well, given the fact that higher moments are factorially suppressed. Nevertheless, one may question whether the higher-twist effects are small for the range of z under consideration. Therefore, in this section, we will fit the data by including the leading power correction using the formula,

$$\mathcal{M}(z, P, \Delta) = \sum_{n=0} \frac{(-izP)^n}{n!} \frac{C_n^{\overline{\text{MS}}}(\mu^2 z^2) \langle x^n \rangle}{C_0^{\overline{\text{MS}}}(\mu^2 z^2)} + \Lambda z^2.$$
 (D1)

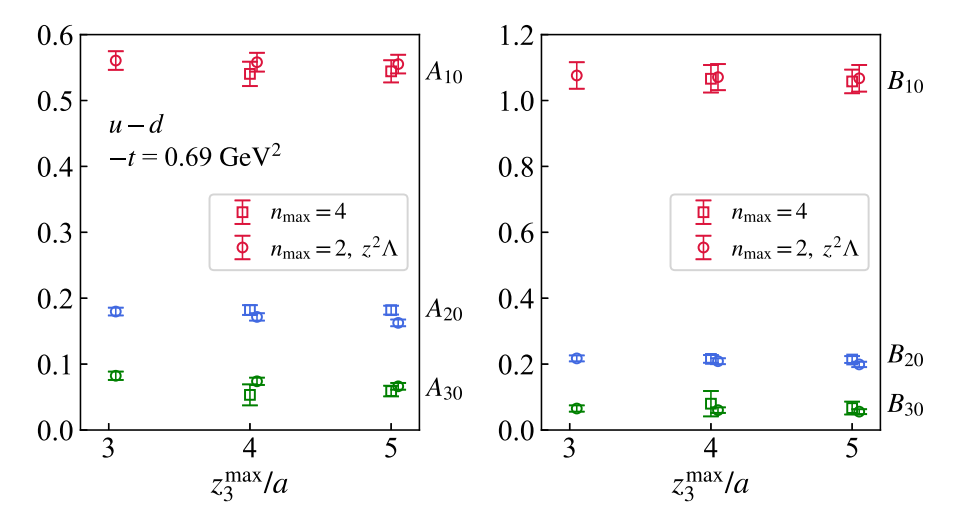


FIG. 20. The first three moments extracted from leading-twist $n_{\text{max}} = 4$ SDF and $n_{\text{max}} = 2$ with $\Lambda^2 z^2$ term are shown as a function of z_{max} for the case of -t = 0.69 GeV².

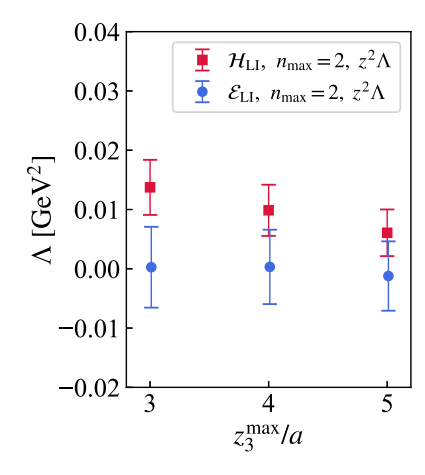


FIG. 21. The Λ term fitted from \mathcal{H}_{LI} and \mathcal{E}_{LI} renormalized matrix elements using Eq. (D1).

Since the fourth and fifth moments are mostly consistent with zero and the fit becomes unstable with additional parameters, we simply truncate the $n_{\rm max}=2$ after adding Λz^2 . For the case of $-t=0.69~{\rm GeV^2}$, we have three different momenta $P_3=0.83$, 1.25 and 1.67 GeV as shown in Fig. 8. In Fig. 20, we show the first three moments extracted from leading-twist $n_{\rm max}=4~{\rm SDF}$ formula and $n_{\rm max}=2$ formula with the Λz^2 term. The fitted Λ term and $\chi^2_{\rm do,f}$ are shown in Figs. 21 and 22.

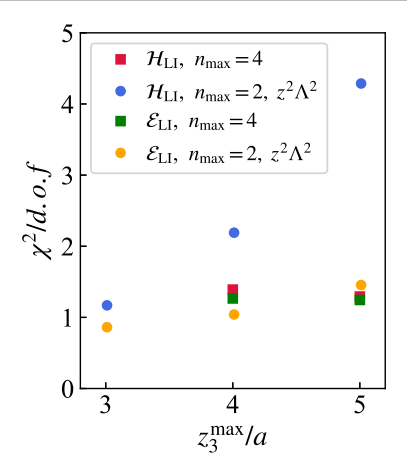


FIG. 22. The $\chi^2/\text{d.o.f}$ of the fit from $n_{\text{max}} = 4$ SDF and $n_{\text{max}} = 2$ with leading higher-twist correction.

We find that in the short distance under consideration, the Λ term is consistent with zero, and moments from different strategies agree with each other, suggesting that higher-twist corrections are negligible. Meanwhile, it can be seen that as the increasing of z_3 , the $\chi^2_{\rm d.o.f}$ of $n_{\rm max}=2$ with the Λz^2 term becomes large while the ones of $n_{\rm max}=4$ are still good. That means the fits including higher moments can better describe the data instead of the leading power correction Λz^2 term.

^[1] D. Müller, D. Robaschik, B. Geyer, F. M. Dittes, and J. Hořejši, Fortschr. Phys. **42**, 101 (1994).

^[2] X.-D. Ji, Phys. Rev. Lett. 78, 610 (1997).

^[3] A. V. Radyushkin, Phys. Lett. B 380, 417 (1996).

^[4] M. Burkardt, Phys. Rev. D 62, 071503 (2000); 66, 119903(E) (2002).

^[5] J. P. Ralston and B. Pire, Phys. Rev. D 66, 111501 (2002).

^[6] M. Diehl, Eur. Phys. J. C **25**, 223 (2002); **31**, 277(E) (2003)

^[7] M. Burkardt, Int. J. Mod. Phys. A 18, 173 (2003).

^[8] M. V. Polyakov and A. G. Shuvaev, arXiv:hep-ph/0207153.

^[9] M. V. Polyakov, Phys. Lett. B 555, 57 (2003).

^[10] M. V. Polyakov and P. Schweitzer, Int. J. Mod. Phys. A 33, 1830025 (2018).

^[11] M. Guidal, M. V. Polyakov, A. V. Radyushkin, and M. Vanderhaeghen, Phys. Rev. D **72**, 054013 (2005).

^[12] S. V. Goloskokov and P. Kroll, Eur. Phys. J. C 42, 281 (2005).

^[13] D. Mueller and A. Schafer, Nucl. Phys. B739, 1 (2006).

^[14] K. Kumerički and D. Mueller, Nucl. Phys. **B841**, 1 (2010).

^[15] G. R. Goldstein, J. O. Hernandez, and S. Liuti, Phys. Rev. D 84, 034007 (2011).

^[16] J. O. Gonzalez-Hernandez, S. Liuti, G. R. Goldstein, and K. Kathuria, Phys. Rev. C 88, 065206 (2013).

^[17] B. Kriesten, P. Velie, E. Yeats, F. Y. Lopez, and S. Liuti, Phys. Rev. D 105, 056022 (2022).

^[18] H. Hashamipour, M. Goharipour, K. Azizi, and S. V. Goloskokov, Phys. Rev. D **105**, 054002 (2022).

^[19] Y. Guo, X. Ji, and K. Shiells, J. High Energy Phys. 09 (2022) 215.

^[20] Y. Guo, X. Ji, M. G. Santiago, K. Shiells, and J. Yang, J. High Energy Phys. 05 (2023) 150.

^[21] H. Hashamipour, M. Goharipour, K. Azizi, and S. V. Goloskokov, Phys. Rev. D 107, 096005 (2023).

^[22] K. Kumericki, S. Liuti, and H. Moutarde, Eur. Phys. J. A 52, 157 (2016).

^[23] D. Mueller, Few-Body Syst. **55**, 317 (2014).

^[24] V. Bertone, H. Dutrieux, C. Mezrag, H. Moutarde, and P. Sznajder, Phys. Rev. D 103, 114019 (2021).

^[25] E. Moffat, A. Freese, I. Cloët, T. Donohoe, L. Gamberg, W. Melnitchouk, A. Metz, A. Prokudin, and N. Sato, arXiv:2303.12006.

^[26] M. Guidal and M. Vanderhaeghen, Phys. Rev. Lett. 90, 012001 (2003).

^[27] A. V. Belitsky and D. Mueller, Phys. Rev. Lett. 90, 022001 (2003).

^[28] A. Pedrak, B. Pire, L. Szymanowski, and J. Wagner, Phys. Rev. D 96, 074008 (2017; 100, 039901(E) (2019).

- [29] G. Duplančić, K. Passek-Kumerički, B. Pire, L. Szymanowski, and S. Wallon, J. High Energy Phys. 11 (2018) 179.
- [30] J.-W. Qiu and Z. Yu, J. High Energy Phys. 08 (2022) 103.
- [31] J.-W. Qiu and Z. Yu, Phys. Rev. D 107, 014007 (2023).
- [32] G. Duplančić, S. Nabeebaccus, K. Passek-Kumerički, B. Pire, L. Szymanowski, and S. Wallon, Phys. Rev. D 107, 094023 (2023).
- [33] P. Hagler, J. W. Negele, D. B. Renner, W. Schroers, T. Lippert, and K. Schilling (LHPC and SESAM Collaborations), Phys. Rev. D 68, 034505 (2003).
- [34] D. Brommel et al. (QCDSF-UKQCD Collaboration), Proc. Sci. LATTICE2007 (2007) 158.
- [35] C. Alexandrou, J. Carbonell, M. Constantinou, P. A. Harraud, P. Guichon, K. Jansen, C. Kallidonis, T. Korzec, and M. Papinutto, Phys. Rev. D 83, 114513 (2011).
- [36] C. Alexandrou, M. Constantinou, S. Dinter, V. Drach, K. Jansen, C. Kallidonis, and G. Koutsou, Phys. Rev. D 88, 014509 (2013).
- [37] M. Constantinou, Proc. Sci. LATTICE2014 (2015) 001.
- [38] J. R. Green, J. W. Negele, A. V. Pochinsky, S. N. Syritsyn, M. Engelhardt, and S. Krieg, Phys. Rev. D 90, 074507 (2014).
- [39] C. Alexandrou, M. Constantinou, K. Hadjiyiannakou, K. Jansen, C. Kallidonis, G. Koutsou, and A. Vaquero Aviles-Casco, Phys. Rev. D 96, 034503 (2017).
- [40] C. Alexandrou, M. Constantinou, K. Hadjiyiannakou, K. Jansen, C. Kallidonis, G. Koutsou, and A. Vaquero Aviles-Casco, Phys. Rev. D 96, 054507 (2017).
- [41] N. Hasan, J. Green, S. Meinel, M. Engelhardt, S. Krieg, J. Negele, A. Pochinsky, and S. Syritsyn, Phys. Rev. D 97, 034504 (2018).
- [42] R. Gupta, Y.-C. Jang, H.-W. Lin, B. Yoon, and T. Bhattacharya, Phys. Rev. D 96, 114503 (2017).
- [43] S. Capitani, M. Della Morte, D. Djukanovic, G. M. von Hippel, J. Hua, B. Jäger, P. M. Junnarkar, H. B. Meyer, T. D. Rae, and H. Wittig, Int. J. Mod. Phys. A 34, 1950009 (2019).
- [44] C. Alexandrou, S. Bacchio, M. Constantinou, J. Finkenrath, K. Hadjiyiannakou, K. Jansen, G. Koutsou, and A. Vaquero Aviles-Casco, Phys. Rev. D 100, 014509 (2019).
- [45] E. Shintani, K.-I. Ishikawa, Y. Kuramashi, S. Sasaki, and T. Yamazaki, Phys. Rev. D 99, 014510 (2019); 102, 019902(E) (2020).
- [46] Y.-C. Jang, T. Bhattacharya, R. Gupta, H.-W. Lin, and B. Yoon (PNDME Collaboration), Proc. Sci. LATTICE2018 (2018) 123.
- [47] G. S. Bali, S. Collins, M. Gruber, A. Schäfer, P. Wein, and T. Wurm, Phys. Lett. B 789, 666 (2019).
- [48] G. S. Bali, S. Collins, M. Göckeler, R. Rödl, A. Schäfer, and A. Sternbeck, Phys. Rev. D 100, 014507 (2019).
- [49] C. Alexandrou et al., Phys. Rev. D 101, 034519 (2020).
- [50] M. Constantinou et al., Prog. Part. Nucl. Phys. 121, 103908 (2021).
- [51] C. Alexandrou et al., Phys. Rev. D 107, 054504 (2023).
- [52] P. Hagler *et al.* (LHPC Collaboration), Phys. Rev. D 77, 094502 (2008).
- [53] X. Ji, Phys. Rev. Lett. 110, 262002 (2013).
- [54] X. Ji, Sci. China Phys. Mech. Astron. 57, 1407 (2014).

- [55] X. Ji, Y.-S. Liu, Y. Liu, J.-H. Zhang, and Y. Zhao, Rev. Mod. Phys. 93, 035005 (2021).
- [56] A. V. Radyushkin, Phys. Rev. D 96, 034025 (2017).
- [57] K. Orginos, A. Radyushkin, J. Karpie, and S. Zafeiropoulos, Phys. Rev. D **96**, 094503 (2017).
- [58] K.-F. Liu and S.-J. Dong, Phys. Rev. Lett. **72**, 1790 (1994).
- [59] V. Braun, P. Gornicki, and L. Mankiewicz, Phys. Rev. D 51, 6036 (1995).
- [60] U. Aglietti, M. Ciuchini, G. Corbo, E. Franco, G. Martinelli, and L. Silvestrini, Phys. Lett. B 441, 371 (1998).
- [61] W. Detmold and C. J. D. Lin, Phys. Rev. D 73, 014501 (2006).
- [62] A. J. Chambers, R. Horsley, Y. Nakamura, H. Perlt, P. E. L. Rakow, G. Schierholz, A. Schiller, K. Somfleth, R. D. Young, and J. M. Zanotti, Phys. Rev. Lett. 118, 242001 (2017).
- [63] Y.-Q. Ma and J.-W. Qiu, Phys. Rev. D 98, 074021 (2018).
- [64] W. Detmold, A. V. Grebe, I. Kanamori, C. J. D. Lin, R. J. Perry, and Y. Zhao (HOPE Collaboration), Phys. Rev. D 104, 074511 (2021).
- [65] H.-W. Lin, J.-W. Chen, S. D. Cohen, and X. Ji, Phys. Rev. D 91, 054510 (2015).
- [66] C. Alexandrou, K. Cichy, V. Drach, E. Garcia-Ramos, K. Hadjiyiannakou, K. Jansen, F. Steffens, and C. Wiese, Phys. Rev. D 92, 014502 (2015).
- [67] J.-W. Chen, S. D. Cohen, X. Ji, H.-W. Lin, and J.-H. Zhang, Nucl. Phys. **B911**, 246 (2016).
- [68] C. Alexandrou, K. Cichy, M. Constantinou, K. Hadjiyiannakou, K. Jansen, F. Steffens, and C. Wiese, Phys. Rev. D **96**, 014513 (2017).
- [69] C. Alexandrou, K. Cichy, M. Constantinou, K. Hadjiyiannakou, K. Jansen, H. Panagopoulos, and F. Steffens, Nucl. Phys. B923, 394 (2017).
- [70] J.-W. Chen, T. Ishikawa, L. Jin, H.-W. Lin, Y.-B. Yang, J.-H. Zhang, and Y. Zhao, Phys. Rev. D 97, 014505 (2018).
- [71] H.-W. Lin, J.-W. Chen, T. Ishikawa, and J.-H. Zhang (LP3 Collaboration), Phys. Rev. D 98, 054504 (2018).
- [72] C. Alexandrou, K. Cichy, M. Constantinou, K. Jansen, A. Scapellato, and F. Steffens, Phys. Rev. Lett. 121, 112001 (2018).
- [73] H.-W. Lin, J.-W. Chen, X. Ji, L. Jin, R. Li, Y.-S. Liu, Y.-B. Yang, J.-H. Zhang, and Y. Zhao, Phys. Rev. Lett. 121, 242003 (2018).
- [74] C. Alexandrou, K. Cichy, M. Constantinou, K. Jansen, A. Scapellato, and F. Steffens, Phys. Rev. D 98, 091503 (2018).
- [75] Y.-S. Liu *et al.* (Lattice Parton Collaboration), Phys. Rev. D **101**, 034020 (2020).
- [76] J.-H. Zhang, J.-W. Chen, L. Jin, H.-W. Lin, A. Schäfer, and Y. Zhao, Phys. Rev. D 100, 034505 (2019).
- [77] R. S. Sufian, J. Karpie, C. Egerer, K. Orginos, J.-W. Qiu, and D. G. Richards, Phys. Rev. D 99, 074507 (2019).
- [78] C. Alexandrou, K. Cichy, M. Constantinou, K. Hadjiyiannakou, K. Jansen, A. Scapellato, and F. Steffens, Phys. Rev. D 99, 114504 (2019).
- [79] T. Izubuchi, L. Jin, C. Kallidonis, N. Karthik, S. Mukherjee, P. Petreczky, C. Shugert, and S. Syritsyn, Phys. Rev. D 100, 034516 (2019).

- [80] B. Joó, J. Karpie, K. Orginos, A. Radyushkin, D. Richards, and S. Zafeiropoulos, J. High Energy Phys. 12 (2019) 081.
- [81] B. Joó, J. Karpie, K. Orginos, A. V. Radyushkin, D. G. Richards, R. S. Sufian, and S. Zafeiropoulos, Phys. Rev. D 100, 114512 (2019).
- [82] Y. Chai et al., Phys. Rev. D 102, 014508 (2020).
- [83] B. Joó, J. Karpie, K. Orginos, A. V. Radyushkin, D. G. Richards, and S. Zafeiropoulos, Phys. Rev. Lett. 125, 232003 (2020).
- [84] M. Bhat, K. Cichy, M. Constantinou, and A. Scapellato, Phys. Rev. D 103, 034510 (2021).
- [85] C. Alexandrou, M. Constantinou, K. Hadjiyiannakou, K. Jansen, and F. Manigrasso, Phys. Rev. Lett. 126, 102003 (2021).
- [86] C. Alexandrou, K. Cichy, M. Constantinou, J. R. Green, K. Hadjiyiannakou, K. Jansen, F. Manigrasso, A. Scapellato, and F. Steffens, Phys. Rev. D 103, 094512 (2021).
- [87] H.-W. Lin, J.-W. Chen, Z. Fan, J.-H. Zhang, and R. Zhang, Phys. Rev. D 103, 014516 (2021).
- [88] Z. Fan, X. Gao, R. Li, H.-W. Lin, N. Karthik, S. Mukherjee, P. Petreczky, S. Syritsyn, Y.-B. Yang, and R. Zhang, Phys. Rev. D 102, 074504 (2020).
- [89] X. Gao, L. Jin, C. Kallidonis, N. Karthik, S. Mukherjee, P. Petreczky, C. Shugert, S. Syritsyn, and Y. Zhao, Phys. Rev. D 102, 094513 (2020).
- [90] H.-W. Lin, J.-W. Chen, and R. Zhang, arXiv:2011.14971.
- [91] J. Karpie, K. Orginos, A. Radyushkin, and S. Zafeiropoulos (HadStruc Collaboration), J. High Energy Phys. 11 (2021) 024.
- [92] C. Alexandrou, M. Constantinou, K. Hadjiyiannakou, K. Jansen, and F. Manigrasso, Phys. Rev. D 104, 054503 (2021).
- [93] C. Egerer, R. G. Edwards, C. Kallidonis, K. Orginos, A. V. Radyushkin, D. G. Richards, E. Romero, and S. Zafeiropoulos (HadStruc Collaboration), J. High Energy Phys. 11 (2021) 148.
- [94] C. Egerer *et al.* (HadStruc Collaboration), Phys. Rev. D 105, 034507 (2022).
- [95] X. Gao, A. D. Hanlon, S. Mukherjee, P. Petreczky, P. Scior, S. Syritsyn, and Y. Zhao, Phys. Rev. Lett. 128, 142003 (2022).
- [96] X. Gao, A. D. Hanlon, N. Karthik, S. Mukherjee, P. Petreczky, P. Scior, S. Shi, S. Syritsyn, Y. Zhao, and K. Zhou, Phys. Rev. D 106, 114510 (2022).
- [97] X. Gao, A. D. Hanlon, S. Mukherjee, P. Petreczky, P. Scior, S. Syritsyn, and Y. Zhao, Proc. Sci. LATTICE2022 (2023) 104.
- [98] F. Yao *et al.* (Lattice Parton Collaboration), arXiv:2208
- [99] S. Bhattacharya, K. Cichy, M. Constantinou, A. Metz, A. Scapellato, and F. Steffens, Phys. Rev. D 102, 034005 (2020).
- [100] S. Bhattacharya, K. Cichy, M. Constantinou, A. Metz, A. Scapellato, and F. Steffens, Phys. Rev. D 102, 114025 (2020).
- [101] S. Bhattacharya and A. Metz, Phys. Rev. D **105**, 054027 (2022).
- [102] S. Bhattacharya, K. Cichy, M. Constantinou, A. Metz, A. Scapellato, and F. Steffens, Phys. Rev. D 104, 114510 (2021).

- [103] J.-H. Zhang, L. Jin, H.-W. Lin, A. Schäfer, P. Sun, Y.-B. Yang, R. Zhang, Y. Zhao, and J.-W. Chen (LP3 Collaboration), Nucl. Phys. B939, 429 (2019).
- [104] J.-H. Zhang, J.-W. Chen, X. Ji, L. Jin, and H.-W. Lin, Phys. Rev. D **95**, 094514 (2017).
- [105] G. S. Bali, V. M. Braun, B. Gläßle, M. Göckeler, M. Gruber, F. Hutzler, P. Korcyl, A. Schäfer, P. Wein, and J.-H. Zhang, Phys. Rev. D 98, 094507 (2018).
- [106] R. Zhang, C. Honkala, H.-W. Lin, and J.-W. Chen, Phys. Rev. D 102, 094519 (2020).
- [107] J. Hua, M.-H. Chu, P. Sun, W. Wang, J. Xu, Y.-B. Yang, J.-H. Zhang, and Q.-A. Zhang (Lattice Parton Collaboration), Phys. Rev. Lett. 127, 062002 (2021).
- [108] W. Detmold, A. V. Grebe, I. Kanamori, C. J. D. Lin, S. Mondal, R. J. Perry, and Y. Zhao (HOPE Collaboration), Phys. Rev. D 105, 034506 (2022).
- [109] J. Hua et al., Phys. Rev. Lett. 129, 132001 (2022).
- [110] X. Gao, A. D. Hanlon, N. Karthik, S. Mukherjee, P. Petreczky, P. Scior, S. Syritsyn, and Y. Zhao, Phys. Rev. D 106, 074505 (2022).
- [111] J.-W. Chen, H.-W. Lin, and J.-H. Zhang, Nucl. Phys. B952, 114940 (2020).
- [112] C. Alexandrou, K. Cichy, M. Constantinou, K. Hadjiyiannakou, K. Jansen, A. Scapellato, and F. Steffens, Phys. Rev. Lett. 125, 262001 (2020).
- [113] H.-W. Lin, Phys. Rev. Lett. 127, 182001 (2021).
- [114] C. Alexandrou, K. Cichy, M. Constantinou, K. Hadjiyiannakou, K. Jansen, A. Scapellato, and F. Steffens, Phys. Rev. D 105, 034501 (2022).
- [115] A. Hannaford-Gunn, K. U. Can, R. Horsley, Y. Nakamura, H. Perlt, P. E. L. Rakow, H. Stüben, G. Schierholz, R. D. Young, and J. M. Zanotti (CSSM/QCDSF/UKQCD Collaboration), Phys. Rev. D 105, 014502 (2022).
- [116] S. Bhattacharya, K. Cichy, M. Constantinou, J. Dodson, A. Metz, A. Scapellato, and F. Steffens, Proc. Sci. LATTICE2021 (2022) 054.
- [117] H.-W. Lin, Phys. Lett. B 824, 136821 (2022).
- [118] S. Bhattacharya, K. Cichy, M. Constantinou, J. Dodson, X. Gao, A. Metz, S. Mukherjee, A. Scapellato, F. Steffens, and Y. Zhao, Phys. Rev. D 106, 114512 (2022).
- [119] M. Constantinou, S. Bhattacharya, K. Cichy, J. Dodson, X. Gao, A. Metz, S. Mukherjee, A. Scapellato, F. Steffens, and Y. Zhao, Proc. Sci. LATTICE2022 (2023) 096.
- [120] S. Bhattacharya, K. Cichy, M. Constantinou, J. Dodson, X. Gao, A. Metz, S. Mukherjee, A. Scapellato, F. Steffens, and Y. Zhao, Proc. Sci. LATTICE2022 (2023) 095.
- [121] P. Shanahan, M. Wagman, and Y. Zhao, Phys. Rev. D 102, 014511 (2020).
- [122] Q.-A. Zhang et al. (Lattice Parton Collaboration), Phys. Rev. Lett. 125, 192001 (2020).
- [123] Y. Li et al., Phys. Rev. Lett. 128, 062002 (2022).
- [124] P. Shanahan, M. Wagman, and Y. Zhao, Phys. Rev. D **104**, 114502 (2021).
- [125] M. Schlemmer, A. Vladimirov, C. Zimmermann, M. Engelhardt, and A. Schäfer, J. High Energy Phys. 08 (2021) 004.
- [126] M.-H. Chu *et al.* (LPC Collaboration), Phys. Rev. D **106**, 034509 (2022).
- [127] K. Cichy and M. Constantinou, Adv. High Energy Phys. 2019, 3036904 (2019).

- [128] M. Constantinou, Eur. Phys. J. A 57, 77 (2021).
- [129] K. Cichy, Proc. Sci. LATTICE2021 (2022) 017.
- [130] K. Cichy, EPJ Web Conf. 258, 01005 (2022).
- [131] K. Cichy et al., arXiv:2304.14970.
- [132] M. Constantinou and H. Panagopoulos, Phys. Rev. D 96, 054506 (2017).
- [133] C. Alexandrou et al., Phys. Rev. D 98, 054518 (2018).
- [134] G. S. Bali, B. Lang, B. U. Musch, and A. Schäfer, Phys. Rev. D 93, 094515 (2016).
- [135] X. Ji, J.-H. Zhang, and Y. Zhao, Phys. Rev. Lett. 120, 112001 (2018).
- [136] J. Green, K. Jansen, and F. Steffens, Phys. Rev. Lett. 121, 022004 (2018).
- [137] T. Ishikawa, Y.-Q. Ma, J.-W. Qiu, and S. Yoshida, Phys. Rev. D 96, 094019 (2017).
- [138] Y.-S. Liu, W. Wang, J. Xu, Q.-A. Zhang, J.-H. Zhang, S. Zhao, and Y. Zhao, Phys. Rev. D 100, 034006 (2019).
- [139] T. Izubuchi, X. Ji, L. Jin, I. W. Stewart, and Y. Zhao, Phys. Rev. D 98, 056004 (2018).
- [140] L.-B. Chen, W. Wang, and R. Zhu, Phys. Rev. Lett. 126, 072002 (2021).
- [141] Z.-Y. Li, Y.-Q. Ma, and J.-W. Qiu, Phys. Rev. Lett. 126, 072001 (2021).

- [142] Y. Ji, F. Yao, and J.-H. Zhang, arXiv:2212.14415.
- [143] Y. Su, J. Holligan, X. Ji, F. Yao, J.-H. Zhang, and R. Zhang, Nucl. Phys. **B991**, 116201 (2023).
- [144] G. Lee, J. R. Arrington, and R. J. Hill, Phys. Rev. D 92, 013013 (2015).
- [145] C. Alexandrou, M. Brinet, J. Carbonell, M. Constantinou, P. A. Harraud, P. Guichon, K. Jansen, T. Korzec, and M. Papinutto, Phys. Rev. D 83, 094502 (2011).
- [146] K. Goeke, M. V. Polyakov, and M. Vanderhaeghen, Prog. Part. Nucl. Phys. 47, 401 (2001).
- [147] M. Burkardt, Nucl. Phys. A735, 185 (2004).
- [148] M. Burkardt, Phys. Rev. D 72, 094020 (2005).
- [149] S. Meissner, A. Metz, and K. Goeke, Phys. Rev. D **76**, 034002 (2007).
- [150] M. Göckeler, P. Hägler, R. Horsley, Y. Nakamura, D. Pleiter, P.E.L. Rakow, A. Schäfer, G. Schierholz, H. Stüben, and J. M. Zanotti (QCDSF and UKQCD Collaborations), Phys. Rev. Lett. 98, 222001 (2007).
- [151] A. Frommer, K. Kahl, S. Krieg, B. Leder, and M. Rottmann, SIAM J. Sci. Comput. 36, A1581 (2014).
- [152] C. Alexandrou, S. Bacchio, J. Finkenrath, A. Frommer, K. Kahl, and M. Rottmann, Phys. Rev. D 94, 114509 (2016).